Atlas of Quasicrystalline Tilings

Clifford A. Reiter
(preprint)

Department of Mathematics, Lafayette College, Easton PA 18042, U.S.A.

Abstract. Tilings are created from root lattices using canonical projection. Like diffraction images, these tilings make the quasicrystaline or crystalline nature of many of these structures clear. These tilings may also be viewed as shadows of lattice sphere packings in *n*-dimensions. The atlas gives many new intriguing quasicrystalline tilings in a systematic way.

AMS classification scheme numbers: 52C23, 52C20, 05B45

1. Introduction

The classification of the crystallographic symmetry groups in 3-dimensional space in the 19th century was a remarkable achievement that was essential to understanding the x-ray diffraction patterns of materials studied in the early part of the 20th century. That, in turn, facilitated the development of molecular chemistry. There was great shock when diffraction patterns that were impossible for crystalline structures were discovered in real materials in 1984 [1]. These materials have become known as quasicrystals. The existence of quasicrystalline materials has increased interest in the mathematical understanding sets of points structured more loosely than in the regular, periodic pattern of lattices. For example, canonical projection from the 5-dimensional integer lattice can be used to give a thorough analysis of Penrose tilings [2]. When Penrose tilings were introduced [3-5], their remarkable aperiodic properties were recognized, but it was not immediately clear that they were not merely a mathematical curiosity.

Our goal is to provide an atlas of tilings resulting from canonical projection for a much broader class of lattices. Such tilings display shadows of the symmetries of the higher dimensional lattices with a visual representation in the plane. Many of these tilings are new and wonderful quasicrystalline patterns. The lattices can also be visually studied by their diffraction patterns; however, apart from translational and forbidden rotation symmetry, it is difficult to directly observe information from the diffraction pattern. The tilings have considerable inherent interest beyond any obvious lattice and rotational structure. Our focus is upon using canonical projection from the root lattices to obtain nonperiodic tilings. Not surprisingly, the integer lattices in other dimensions behave most like the lattice that generates Penrose tilings while the other root lattice produce quite different, but equally remarkable tilings.

In recent years, root lattices have become more important because of their relation to codes and sphere packings [6]. Modern theories of fractal space-time have highlighted the importance of irregular structures and high dimensional lattices have played an important role in modern physics [7-11]. Thus, we expect the atlas presented here to not

E-mail address: reiterc@lafayette.edu

only be of interest to investigators of tilings but also to those interested in studying sphere packings and other applications of high dimensional lattices themselves.

We understand that in many ways our task is hopeless. There are infinitely many root lattices and even for a single one, say the 5-dimensional integer lattice commonly used to produce Penrose tilings, it is well known that uncountably many such tilings may be created [2]. Moreover, special cases and new generic types appear for special types of "offset" used in the canonical projection. However, the same local configurations appear in many of the variations. The forbidden crystalline symmetries which appear are highlighted by the projection used; so while they are a feature of the lattice, the fact that that aspect of the lattice symmetry is visible depends upon the choice of projection. In any case, the tilings give visual shadows of the higher dimensional lattices which are worthwhile, even while we recognize the impossibility of conveying all the features of such a lattice with a planar tiling.

Quasicrystals are recognized by their diffraction patterns which exhibit symmetry impossible for a crystallographic pattern. The 3-dimensional crystallographic groups and diffraction theory are described in [12-14] and generalizations to 4-dimesions are given in [15]. A wonderful visual atlas of diffraction patterns appears in [16]. That atlas provides a guide to the diffraction patterns produced by simple masks as well as exploring complex masks including those related to crystallographic patterns. A chapter in [2] considers diffraction patterns for tilings, including a few nonperiodic tilings.

An important general introduction to tilings is [17]; however, that book was written before physical quasicrystals were discovered. Radin [18] discusses the theory of tilings from a post quasicrystalline viewpoint. Nonetheless, [17] does discuss nonperiodic tilings and aperiodic tilings. Aperiodic tilings are tilings whose tiles only give nonperiodic tilings. While aperiodic tilings are remarkable, see also [2, 19], we are interested in the nonperiodic tilings arising from canonical projection, which we call quasicrystalline tilings.

We note that a handful of quasicrytalline tilings, created from integer lattices, appear at [20]. Patterns arising from the A_4 root lattice are analyzed in [21]. Generalizations of Voronoi tilings and their duals have also been used to create remarkable quasicrystalline tilings [22-23] and a substantial theory for the tilings that arise when the projections are quadratic has been developed [24-25].

2. Canonical Projection

The Voronoi cell around a point in a collection of points is the set of points in space that are at least as close to the given point as any other point in the collection. The Voronoi cells decompose space into neighborhoods around the collection of points in a natural way. Figure 1 shows the Voronoi cells around a Penrose configuration of points. Notice each point is surrounded by a polygon forming its Voronoi cell and each edge is a segment on a bisector between two points. The Voronoi cells for a lattice must be congruent since each point in a lattice has a neighborhood looking like any other. Thus, the Voronoi cells for a lattice are a polytope that tile space. Since the point set in Figure 1 is not a lattice, the Voronoi tiling seen there is more complicated.

Canonical projection of a lattice in $\Re^n$ is based upon the idea of decomposing $\Re^n$ in terms of orthogonal spaces E and $E^\perp$ and projecting select portions of the lattice in

$\Re^n$ onto *E*. In particular, some compact set, *C*, in $E^\perp$ is chosen. The "canonical" choice for *C* is the projection of Voronoi cell of the origin in $\Re^n$, relative to the lattice, as projected onto $E^\perp$. We also shift (translate) the points before we project and test them; one can equivalently describe the compact set *C* as shifted, but for convenience, we do our shift in $\Re^n$. The points which are projected onto *E* are the points of the lattice which map to *C* under shift and projection to $E^\perp$. In other words, the preimage of *C* corresponds to a cylinder in $\Re^n$, compact in some directions and unbounded in others. The points of the lattice in $\Re^n$ which are in that cylinder are projected onto *E*.

Figure 2 illustrates canonical projection in a simpler situation than we will use, but it serves as a useful overview of the process. In the figure, the orthogonal spaces *E* and $E^\perp$ are the marked lines and together they generate $\Re^2$. A compact set *C* in $E^\perp$ is marked in black. The set *C* defines a cylinder in $\Re^2$ which lies between the dashed lines. Some of the integer lattice points lie in the cylinder—these are marked as points with gray centers. Others lattice points lie outside the cylinder—these are marked as points with hollow centers. Those that are in the cylinder are projected onto E along dotted lines to points marked with black circles. The result of canonical projection of the lattice is that point set in *E*.

The projections we use are not as simple. We are interested in the case when *E* is 2-dimensional and seek to connect the projected points with edges to give a tiling. Moreover, the compact sets we use tend to be quite complex. Our last example involves a polytope with more than 40,000 facets as the compact set *C*.

Usually the shift used in the projection and the subspaces *E* and $E^\perp$ are chosen so that *E* does not meet any faces of the shifted Voronoi cell; this avoid singular cases. When singular cases are avoided and the lattice is integral, there is a general theory that concludes that the projected point set is nonperiodic [2, 26].

In order to obtain a tiling, we connect two projected vertices in *E* by an edge if the corresponding vertices in the cylinder (in $\Re^n$) differ by a facet vector of the Voronoi cell. That is, we can imagine the selected lattices points in the cylinder giving a vertex set; vertices are connected by an edge if they differ by a facet vector of the Voronoi cell; the set of vertices and edges gives a graph with a particular geometric representation in $\Re^n$. The tiling we seek is the projection of that geometric graph onto *E*. There is no reason to believe ahead of time that the tiling will only use a small number of distinct tiles; nor have we specified enough to guarantee that edges won't cross. Thus, additional vertices, corresponding to the intersections, would need to be introduced in order to make some of the images we create into formal tilings. As we have noted, in the nonsingular integral cases we expect nonperiodic tilings, we call these quasicrystalline tilings. In many cases even the nonperiodic tilings are quite regular, but in every case they are a shadow of the generating lattice in $\Re^n$ and exhibit some of its symmetry.

3. Root Lattices

The root lattices may be characterized various ways, but they consist of three infinite families, Z^n, D_n and A_n, where *n* denotes the dimension of the lattice, along with three special lattices in a family: E_6, E_7, and E_8. For a detailed enumeration of many of their properties, see [6]; the classic book [27] also describes many of their properties,

especially those related to the polytopes related to these constructions. We will content ourselves to describing the properties we will use and focus our examples on $3 \le n \le 8$, although we will consider some slightly higher dimensional cases for Z^n.

The integer lattice Z^n is generated by the rows of the *n* by *n* identity matrix and the Voronoi cell around the origin has 2*n* facets, half a unit from the origin, and orthogonal to the generators and their opposites. The covering radius for a lattice is the minimal radius such that the union of the spheres of that radius centered at the lattice points will cover space. The covering radius for Z^n is $R = \frac{\sqrt{n}}{2}$.

The lattice D_n is $\{(x_1, x_2, \cdots, x_n) \in Z^n \mid x_1 + x_2 + \cdots + x_n \text{ is even}\}$. This lattice is called the checkerboard lattice since every alternate vertex of Z^n is included. It is generated by the rows of the following matrix.

$$\begin{pmatrix} -1 & -1 & 0 & 0 & \cdots & 0 & 0 \\ 1 & -1 & 0 & 0 & \cdots & 0 & 0 \\ 0 & 1 & -1 & 0 & \cdots & 0 & 0 \\ \vdots & \vdots & \vdots & \vdots & \ddots & \vdots & \vdots \\ 0 & 0 & 0 & 0 & \cdots & 1 & -1 \end{pmatrix}$$

The Voronoi cells are generated by the $2n(n + 1)$ permutations of $(\pm 1, \pm 1, 0, \cdots, 0)$ and the covering radius is $R = \frac{\sqrt{n}}{2}$ for $n > 3$ and R=1 for n = 3.

The lattice A_n is $\{(x_1, x_2, \cdots, x_{n+1}) \in Z^{n+1} \mid x_1 + x_2 + \cdots + x_{n+1} = 0\}$. It is generated by the rows of:

$$\begin{pmatrix} -1 & 1 & 0 & 0 & \cdots & 0 & 0 \\ 0 & -1 & 1 & 0 & \cdots & 0 & 0 \\ 0 & 0 & -1 & 1 & \cdots & 0 & 0 \\ \vdots & \vdots & \vdots & \vdots & \ddots & \vdots & \vdots \\ 0 & 0 & 0 & 0 & \cdots & -1 & 1 \end{pmatrix}$$

The Voronoi cells are generated by the $(n + 1)(n + 2)$ vectors that consist of the permutations of $(1, -1, 0, \cdots, 0)$. The covering radius is $R = \sqrt{\frac{\left\lfloor \frac{n+1}{2} \right\rfloor \left(n + 1 - \left\lfloor \frac{n+1}{2} \right\rfloor \right)}{n+1}}$ where $\left\lfloor \frac{n+1}{2} \right\rfloor$ is the floor of the quotient.

The lattice E_8 is $\{(x_1, x_2, \cdots, x_8) \mid \text{all } x_i \in Z \text{ or all } x_i \in Z + \frac{1}{2} \text{ and } x_1 + x_2 + \cdots + x_8 \equiv 0 \bmod 2\}$. It is generated by the rows of the following matrix.

$$\begin{pmatrix} 2 & 0 & 0 & 0 & 0 & 0 & 0 & 0 \\ -1 & 1 & 0 & 0 & 0 & 0 & 0 & 0 \\ 0 & -1 & 1 & 0 & 0 & 0 & 0 & 0 \\ 0 & 0 & -1 & 1 & 0 & 0 & 0 & 0 \\ 0 & 0 & 0 & -1 & 1 & 0 & 0 & 0 \\ 0 & 0 & 0 & 0 & -1 & 1 & 0 & 0 \\ 0 & 0 & 0 & 0 & 0 & -1 & 1 & 0 \\ \frac{1}{2} & \frac{1}{2} & \frac{1}{2} & \frac{1}{2} & \frac{1}{2} & \frac{1}{2} & \frac{1}{2} & \frac{1}{2} \end{pmatrix}$$

In computational practice, we use a rescaled version of the lattice in order to maintain integral entries.

The E_6 and E_7 lattices appear as sublattices of E_8; E_7 may be described by $E_7 = \{(x_1, x_2, \cdots, x_8) \in E_8 \,|\, x_1 + x_2 + \cdots + x_8 = 0\}$ and E_6 may be described by $E_6 = \{(x_1, x_2, \cdots, x_8) \in E_8 \,|\, x_1 + x_8 = x_2 + \cdots + x_7 = 0\}$. The generating matrices for these lattices may be found in [6]. The Voronoi cells of the E_6, E_7 and E_8 lattices have 72, 126, and 240 facets. The projections are far more complex as we will see in Section 10. The covering radii for these lattices are $R = \sqrt{\frac{4}{3}}, \sqrt{\frac{3}{2}}$, and 1, respectively.

4. Quasicrystalline Projection

In order to obtain local symmetry in our tilings we select the canonical projection in a way so that certain symmetrically related lattice points remain related. In particular, we select E in $\Re^n$ so that it is preserved by a certain n-fold rotation.

The most commonly used subspaces E and $E^\perp$ that generate Penrose tilings are defined as follows. The subspace E of $\Re^5$ is generated by the two vectors:

$$\vec{u}_1 = (\cos(0\pi/5), \cos(2\pi/5), \cos(4\pi/5), \cos(6\pi/5), \cos(8\pi/5)),$$
$$\vec{u}_2 = (\sin(0\pi/5), \sin(2\pi/5), \sin(4\pi/5), \sin(6\pi/5), \sin(8\pi/5)).$$

The subspace $E^\perp$ is generated by the three vectors:

$$\vec{u}_3 = (\cos(0\pi/5), \cos(4\pi/5), \cos(8\pi/5), \cos(12\pi/5), \cos(16\pi/5)),$$
$$\vec{u}_4 = (\sin(0\pi/5), \sin(4\pi/5), \sin(8\pi/5), \sin(12\pi/5), \sin(16\pi/5)), \text{ and}$$
$$\vec{u}_5 = (1,1,1,1,1).$$

The five vectors taken together, $\{\vec{u}_1, \vec{u}_2, \cdots, \vec{u}_5\}$, form an orthogonal coordinate system.

We generalize the above choice of subspaces and coordinate system to $\Re^n$, for $n \geq 3$, as follows. Let E be generated by the two vectors:

$$\vec{u}_1 = (\cos(0\pi/n), \cos(2\pi/n), \cos(4\pi/n), \cdots, \cos(2(n-1)\pi/n))$$
$$\vec{u}_2 = (\sin(0\pi/n), \sin(2\pi/n), \sin(4\pi/n), \cdots, \sin(2(n-1)\pi/n)).$$

Furthermore, let $E^\perp$ be generated by the vectors:

$$\vec{u}_{2j-1} = (\cos(0\pi j/n), \cos(2\pi j/n), \cos(4\pi j/n), \cdots, \cos(2j(n-1)\pi/n)),$$
$$\vec{u}_{2j} = (\sin(0\pi j/n), \sin(2\pi j/n), \sin(4\pi j/n), \cdots, \sin(2j(n-1)\pi/n))$$

for $2 \le j \le \left\lceil \frac{n-2}{2} \right\rceil$. Also $\vec{u}_n = (1,1,1,\cdots,1)$ and when *n* is even we also use $\vec{u}_{n-1} = (1,-1,1,-1,\cdots,1,-1)$.

We can check that $\{\vec{u}_1, \vec{u}_2, \cdots, \vec{u}_n\}$ forms an orthogonal coordinate system. Now let $\mathrm{r}(x_1, x_2, \cdots, x_n) = (x_2, x_3, \cdots, x_n, x_1)$ which is a function that gives an *n*-fold rotation of coordinates. We see that r fixes the last vector in that basis, $\mathrm{r}(\vec{u}_n) = \vec{u}_n$ and we claim that $\mathrm{r}(E) = E$. We show the claim by observing the linearity of r and showing that the image of $\vec{u}_1$ and $\vec{u}_2$ under r is a linear combination of $\vec{u}_1$ and $\vec{u}_2$ and hence in *E*. If we write $\vec{u}_1 = \left\langle \cos(\frac{2k\pi}{n}) \right\rangle_{0 \le k \le n-1}$ and likewise $\vec{u}_2 = \left\langle \sin(\frac{2k\pi}{n}) \right\rangle_{0 \le k \le n-1}$, we see the image of $\vec{u}_1$ under r is:

$$\begin{aligned} r(\vec{u}_1) &= \left\langle \cos(\frac{2(k+1)\pi}{n}) \right\rangle_{0 \le k \le n-1} \\ &= \left\langle \cos(\frac{2k\pi}{n} + \frac{2\pi}{n}) \right\rangle_{0 \le k \le n-1} \\ &= \left\langle \cos(\frac{2k\pi}{n})\cos(\frac{2\pi}{n}) - \sin(\frac{2k\pi}{n})\sin(\frac{2\pi}{n}) \right\rangle_{0 \le k \le n-1} \\ &= \cos(\frac{2\pi}{n})\vec{u}_1 - \sin(\frac{2\pi}{n})\vec{u}_2 \end{aligned}$$

which is in *E* as claimed. A similar argument shows the same for the image of $\vec{u}_2$. Thus we have chosen *E* so that if it contains a lattice point, then the rotations of the lattice point under r will also be in *E*. If the lattice is mapped to itself by r, and the compact set is symmetric under r, then this is enough to give global *n*-fold symmetry to the tiling. Even without C being completely symmetric, there are fragments of the symmetry given locally that form the quasicrystalline nature of the structure.

The projection of a unit hypercube in $\Re^5$ onto *E* is shown in Figure 3. Notice that 31 vertices appear; only the central pair of vertices corresponds to a duplicate. Edges which could be used as a local configuration in a Penrose tiling are shown emboldened.

Figure 4 shows a portion of a typical Penrose tiling (its set of vertices is the same as appeared in Figure 1). This is constructed using the standard Voronoi cell around the origin as the compact set with a suitable shift—along with our standard spaces *E* and $E^{\perp}$, described above. The shift used to generate Figure 4 is special in that only certain vertex configurations are possible. In the next section we discuss several different types of shifts that we will use, along with briefly exploring other variations.

5. Variation of the Compact Set

We have already mentioned that shifting is an important way to change the compact set in $E^{\perp}$ used to create the tiling. In addition, we can increase or decrease the diameter of the Voronoi cell and even choose the compact set to have nothing to do with projected Voronoi cells. We will primarily utilize the Voronoi cell with one of the following types of shifts. We describe each shift relative to the basis of unit vectors $\langle \hat{u}_1, \hat{u}_2, ..., \hat{u}_n \rangle$ where

$\hat{u}_i$ is the unit vector in the $\vec{u}_i$ direction. That is, points in $\Re^n$ are shifted by addition of $\sum_{i=1}^{n} \alpha_i \hat{u}_i$ before they are projected to $E^{\perp}$, where we test whether the image is in the compact set (canonically the image of the Voronoi cell around the origin). Table I shows the six types of shifts. The covering radius of the lattice is denoted by *R* and ν is the expansion factor of the Voronoi cell (usually $\nu = 1$). The "*"s correspond to random decimal numbers created with a fixed seed. Further details are given in Section 10, but for now a "*" should be considered a generic, and hence nonsingular, shift.

s_i	$\langle \alpha_1, \alpha_2, \cdots, \alpha_n \rangle$
s_0	$\langle 0,0,*,*,\cdots,*,* \rangle$
s_1	$\langle 0,0,*,*,\cdots,*,R\nu \rangle$
s_2	$\left\langle 0,0,*,*,\cdots,*,\frac{R\nu}{2} \right\rangle$
s_3	$\langle 0,0,0,\cdots,0,R\nu \rangle$
s_4	$\left\langle 0,0,0,\cdots,0,\frac{R\nu}{2} \right\rangle$
s_5	$\langle 0,0,0,\cdots,0,0 \rangle$

Table I. Six types of shifts used on Voronoi cells.

The Penrose tiling shown in Figure 4 was created using a shift of type s_1. Since the covering radius is $\frac{\sqrt{5}}{2}$ and that is half the length of the body diagonal of the 5-cube, this corresponds to "sum condition being one-half" that is used to distinguish Penrose projections from some of its generalizations [2]. The choice of $\alpha_1 = \alpha_2 = 0$ in all cases corresponds to the fact that these coordinates correspond to translations in *E* and don't affect the underlying tiling.

Figure 5 shows the diminished tiling that occurs when the Voronoi cell used for Figure 4 is contracted by a factor of 0.9. Likewise, Figure 6 shows the enlarged tiling corresponding to expansion factor of 1.1. Notice the large number of crossing edges visible and various substantial portions of hypercubes (recall Figure 3) may be observed. An animation showing the evolution of the tiling as the expansion factor varies is available at [28].

We may also consider test sets which have nothing to do with the Voronoi cells. For example, if we use a unit 3-cube in $E^{\perp}$ that is contracted by a factor of 0.7251 as the compact test set, the resulting tiling is shown in Figure 7. Notice the unattached edges. However, if a unit 3-sphere that is contracted by a factor of 0.861 is used as the compact set in $E^{\perp}$, the resulting tiling is shown in Figure 8. Notice the similarities to Figure 5, except that a wider range vertex configurations are allowed. Animations corresponding to the changes in contraction factor may be found at [28].

We now consider the result of different shifts corresponding to the ordinary Voronoi cell. Figure 9 shows the result of an s_0 shift. Notice the large number of 10-fold

vertex configurations (forbidden in Penrose tilings). Like the tiling produced by most of the shifts, this is a generalization of a Penrose tiling. The rhombic tiles are shown in different colors depending upon their shape and orientation in the plane. Notice the striking appearance of the regions consisting of the thinner rhombs. The result of an s_2 shift is shown in Figure 10. Again, Penrose-tiling forbidden configurations appear, although 10-fold configurations are not visible. The result of an s_3 shift is shown in Figure 11. Here the shift allows more edges than produce rhombs; thus there are many crossing edges and the tiling appears less regular than for the other shifts. However, there is a 10-fold rotational symmetry.

We recall that the last α-coordinate of the shift corresponds to the unit vector in the $\vec{u}_n = (1,1,1,\cdots,1)$ direction that is preserved by permutations of coordinates, including rotations of coordinates such as $\mathrm{r}(x_1, x_2, \cdots, x_n) = (x_2, x_3, \cdots, x_n, x_1)$. If all the other α-coordinates of the shift are zero, then the compact set will be symmetric with respect to r (describing the geometry as though the set *C* is shifted). The shifts s_3, s_4 and s_5 all have that property and hence give globally symmetric tilings if the lattice also is symmetric with respect to r. All of the root lattices have the symmetry with respect to r except E_6.

The result of an s_4 shift is shown in Figure 12. There the global 5-fold symmetry is fairly apparent; look along the 5 lines emanating from the center, where 5-rhombs meet. This is a Penrose tiling with global rotational symmetry. The result of an s_5 shift is shown in Figure 13. It corresponds to no shift and the extra symmetry results. In particular, 10-fold vertex configurations appear as does a global 10-fold symmetry. The site [28] also shows animations of tilings morphing from one shift type to another.

Before turning to our atlas which forms the main body of the paper, we reemphasize the significance of the choice of spaces *E* and $E^{\perp}$. Figure 14 shows the projection of the lattice points from Z^5 using a random choice for the subspaces *E* and $E^{\perp}$, so there is no reason to expect 5-fold local symmetry. Notice the tiling is complicated, but appears to be periodic. This is quite different from Figures 3-13 that arise from the same lattice. Figure 15 shows the diffraction pattern for the tiling in Figure 4. Notice the 10-fold symmetry which is forbidden for crystalline structures; hence the Penrose tiling we saw in Figure 4 is quasicrystalline. The diffraction pattern in Figure 15 is shown with contrast optimized, as described for diffraction experiments in [29], in order to highlight the symmetry. If linear contrast is used instead, the discreteness of the pattern becomes apparent but it is more difficult to observe the forbidden symmetry. In contrast, Figure 16 shows the diffraction pattern for the tiling in Figure 14. We see that while the diffraction pattern shows a distinct pattern, there is not forbidden rotational symmetry. Thus our standard choice of *E* and $E^{\perp}$ described in the previous section plays an important role the quasicrytalline nature of our tilings.

6. Tilings from the Integer Lattice, Z^n, $3 \le n \le 10$.

The tilings that arise via canonical projection are most regular for the integer lattice. Low, "crystalline" dimensions, *n* = 3, 4, 6, give rise to periodic structures, but non-periodic tilings are typical for higher dimensions.

Using our standard projections, we see the tiling arising from Z^3 is either a periodic 6-fold symmetric rhomb tiling (s_0, s_2, s_4, s_5) or a periodic equilateral triangular tiling obtained by dividing each rhomb in half. Figure 17 shows the rhomb tiling

associated with s_0. The tilings that arise from the Z^4 lattice give rise to a ordinary square tiling for all the shifts. In the previous section we considered the rich variety of non-periodic tilings that arise from the Z^5 lattice and will say no more about them here.

The Z^6 lattice gives rise to several different periodic tilings. These include regular tiling by equilateral triangles (s_3), the rhomb tiling like that seen in Figure 17 (s_2, s_4), and a tiling which is a decomposition of that tiling by a factor of two (s_1, s_5) and a slightly more complicated periodic rhomb tiling from an s_0 shift; see Figure 18.

The integer lattice Z^7 gives nonperiodic tilings. Figure 19 shows a generic tiling from a shift of type s_0. Figure 20 shows an nonperiodic tiling arising from an s_0 shift on the Z^8 lattice. The simplicity of the tiling is in contrast to its irregularity. The tiling arising from an s_4 shift is even more subtle; it gives a 8-fold symmetric tiling that must be non-periodic. However, notice how periodic it appears to be at a glance; see Figure 21.

The Z^9 lattice also give rise to nonperiodic tilings. Figure 22 shows striking 9-fold central symmetry arising from an s_4 shift. Figure 23 shows a generic nonperiodic tiling arising from an s_4 shift on Z^{10}.

7. Tilings from the Checkerboard Lattice, D_n, $3 \le n \le 8$.

Like the integer lattice, the checkerboard lattice gives rise to periodic tilings when n = 3, 4, 6. However, the tilings arising from the checkerboard lattice are far less regular in all cases. Figure 24 shows the s_0 shift tiling arising from D_3. Notice the hexagonal regions encased in triangular scaffolding. This tiling is close to being a 3-grid with some extra edges.

Figure 25 shows a square tiling arising from the s_0 shift with alternate squares bisected diagonally — alternating between left and right diagonals as might be expected as the shadow of a checkerboard lattice. All the other shifts give similar results.

The D_5 lattice gives remarkable tilings that are as rich as those from the Z^5 lattice. Here Figure 26 shows the s_0 shift tiling, Figure 27 shows the s_3 shift, and Figure 28 shows the s_5 shift. In all of these the local 5-fold symmetry is apparent. Figure 26 uses color to show the wide variation in the tile shapes in the tiling. The tiles have been colored using the techniques in [30]. Figure 27 shows a similar tiling, except stars within stars have a dramatic appearance and the tiles are not colored. In Figure 28 paths of triangles and rhombs form the low density regions and these are reminiscent of the multigrid construction of Penrose tilings, although the gridlines are interrupted and intertwine in an intriguing manner. The dense regions in that figure contain many stars within pentagons.

The D_6 lattice gives rise to a variety of periodic tilings. This includes rectangles with alternate crossovers, rhombs, triangles and other tilings. Figure 29 shows a tiling arising from s_1 (almost a multi-grid).

Figure 30 shows the irregular s_1 based tiling for D_7. The role of 7-gons is apparent, but the connections between 7-gons seem tenuous and thin. The D_8 based tilings are quite varied. Some appear thin and tenuous like Figure 30. Others are rather regular; for example, see Figure 31 which is produced by the s_3 shift.

We have seen that the D_n tilings are not as regular as the integer lattices. Those that are close to being multi-grids, contain exceptional edges. However the variation in density we observe in most of the tilings is not unexpected given the every-other vertex configuration and increased complexity of the Voronoi cell for the underlying lattice.

8. Tilings from the Lattice A_n, $3 \le n \le 8$.

The lattice A_n is embedded in $\Re^{n+1}$ and hence we find the expected periodic tilings when n = 3, 5. Like Figure 25 which we saw for D_4, a bisected square tiling results from A_3 using the s_0 shift. Using other shifts on A_3 gives similar tilings.

The A_4 lattice gives rise to tilings (nearly multi-grid) with many local 5-fold symmetric spots and some pentagons and stars. The s_3, s_4 and s_5 shifts (which are the same since the last α-coordinate has not impact for the A_n tilings) have some global rotational symmetry. If we contract the Voronoi cell by a factor of 0.5 and use an s_0 shift, the tiling shown in Figure 32 results. Notice the 5-fold local symmetry is quite clear.

Figure 33 shows the hexagonal tiling resulting from A_5 using an s_0 shift. Simple rhomb tilings appear for other shifts. The A_6 tilings are very irregular. Figure 34 shows the tiling resulting from the s_5 shift. Here 14-fold rotational symmetry appears along with 7-gons. Figure 35 is the tiling using s_5 and the expansion factor 1.1 giving rise to a remarkably regular 8-fold symmetric tiling. Figure 36 shows an A_8 based tiling using an s_0 shift and 1.2 expansion factor. Note the irregularity and the physical quasicrystal-like appearance.

Like the previous families, the A_n family of lattices give rise to a wide variety of tilings. However, they appear to typically be less regular than those generated by Z^n or D_n.

9. Tilings from the Lattices E_6, E_7, and E_8.

The representation of the lattices we use for the E_n lattices are all embedded in $\Re^8$. Hence they are expected to typically be nonperiodic tilings. The ordinary Voronoi cells are too small to generate a connected set of edges, hence we use an expansion factor in order to obtain interesting tilings. Figure 37 shows the tiling for E_6 using an s_3 shift and an expansion factor of 1.9. The tiling with s_0 shifts has slightly less symmetry and fewer edges. However, the lattice is not symmetric with respect to rotations of coordinates, hence the lack of 8-fold rotational symmetry.

The E_7 lattice does have symmetry with respect to rotation of coordinates. Thus we don't have 8-fold rotational symmetry for an s_2 shift, see Figure 38. This tiling uses an expansion factor of 1.9.

The E_8 lattice has quite a bit of symmetry, including the rotational symmetry when the shift is only in the u_8 direction. Figure 39 shows the tiling for for an s_3 shift and an 2.0 expansion factor. Notice the global symmetry and the rich structure of the tiling. The tiles are colored according to [30]. Lastly, Figure 40 shows the E_8 tiling for an s_2 shift and an expansion factor of 2.15. Many locally 8-fold symmetric configurations are apparent and the physical quasicrystalline quality pervades the image.

10. Computations

We will comment upon three phases of our computations. These are computing the projection of the central Voronoi cell, selecting the shifts, and locating the vertices which give rise to the tilings.

In Section 3 we saw generator matrices for the root lattices. The Voronoi cell may be computed by finding the closure of the set of generators under the operation of

reflection across the hyperplanes defined by the generators. Each of the resulting vectors corresponds to a normal to a facet of the Voronoi cell of the origin. The facet is half the length of the vector from the origin. Our construction uses the fact that all the generators of a root lattice have the same length although this is not essential for canonical projection.

Next, the *n*-3 dimensional faces of the Voronoi cell are enumerated by considering all of the $\binom{n}{3}$ ways of selecting three facets. The projection of these faces into $E^{\perp}$ corresponds either to a *n*-3 dimensional affine hyperplane in $E^{\perp}$ (a facet) or it is a degenerate face. We disgard the degenerate faces and select the affine hyperplane furthest from the origin in each projected facet direction. For testing purposes, we only take one of each opposite pair. Hence, the number shown in the last column of Table II is the number of inequalities that must be tested in order to determine whether the projection of a point is in the projection of the Voronoi cell for the integer lattice. Remember, the projections we are using have special symmetry, so the projected Voronoi cells are not expected to be "generic". Table III shows the analogous information for the checkerboard lattice, Table IV for the A_n lattices, and Table V for the E_n lattices.

The programming language that we used for our constructions was Jsoftware [31]. The shifts that we used were generated with its random number generator using the default random seed and generating four digit numbers. For example, the s_0 shift used to create Figure 9, is, in α-coordinates, given by the following list of 4 decimal place random numbers 0 0 0.1315 0.7556 0.4586 (remember, we always take the first two α-coordinates to be 0).

n	# facets in $\Re^n$	# *n*-3 faces in $\Re^n$	half of # facets in $E^{\perp}$
3	6	20	1
4	8	56	2
5	10	120	10
6	12	220	11
7	14	364	35
8	16	560	36
9	18	816	84
10	20	1140	85
11	22	1540	165
12	24	2024	166

Table II. The face counts for canonical Voronoi cell for the Z^n lattice and its projections.

n	# facets in $\Re^n$	# *n*-3 faces in $\Re^n$	half of # facets in $E^{\perp}$
3	12	220	1
4	24	2024	4
5	40	9880	100
6	60	34220	199
7	84	95284	2261
8	112	227920	3180

Table III. The face counts for canonical Voronoi cell for the D_n lattice and its projections.

n	# facets in $\Re^{n+1}$	# n-2 faces in $\Re^{n+1}$	half of # facets in $E^{\perp}$
3	12	220	1
4	20	1140	5
5	30	4060	34
6	42	11480	189
7	56	27720	530
8	72	59640	1668

Table IV. The face counts for canonical Voronoi cell for the A_n lattice and its projections.

n	# facets in $\Re^8$	# 5-faces in $\Re^8$	half of # facets in $E^{\perp}$
6	72	59640	579
7	126	325500	3957
8	240	2275280	22169

Table V. The face counts for canonical Voronoi cell for the E_n lattice and its projections.

Lastly we comment upon our strategy for finding the lattice points that project to the compact set in $E^{\perp}$. First, testing a single lattice point may require testing many inequalities. The most difficult case that we completed was for E_8 where more than 22,000 inequalities must be tested for each considered lattice point. If we simply tested each lattice point using a fixed range of integers for coefficients of the generators, the computation quickly becomes intractable. Limiting the coefficients to ± 10 would lead to $21^8 \approx 3.8 \times 10^{10}$ lattice points to test for the eight dimensional case. This is too many points and in reality we want more than ± 10 for our range. Instead, we begin with a brute force search on a very small, ± 1, region and identify which lattice points were acceptable. We then consider all the neighbors (using the normals to the Voronoi cell) of the good points and, after removing those that are duplicates and those that have already been tested, we test the remaining neighbors. Note that using a ± 1 sense of neighbor may gives rise to $3^8 = 6561$ neighbors for a single point in 8-dimensional space. This search strategy can not locate unconnected components of the graph in the lattice space, unless the components touch the initial test cell. Nonetheless, this search strategy worked well for us in practice and allowed us to avoid brute force testing of lattice points far from the cylinder of interest.

11. Conclusions

Canonical projection was used create tilings that have local symmetry that is forbidden by the crystallographic restriction for periodic structures. We have seen that there is a natural way to create projections similar to those used for creating Penrose tilings in any dimension. We also have seen several types of shifts and other variations on compact set that give different qualitative behaviors. We have seen many illustrations of remarkable quasicrystalline tilings that result from canonical projection for the root lattices: Z^n, D_n, A_n and E_n. These may be viewed as shadows of root lattice packings. We have seen that the integer lattice gives rise to the tilings most similar to the Penrose tilings, yet the others yield equally intriguing tilings.

Acknowledgment
Conversations with Derek Smith, especially regarding construction of the Voronoi cells for root lattices, were most helpful.

References

[1] Shechtman D, Blech I, Gratias D, Cahn JW. Metallic phase with long-range orientational order and no translational symmetry. Physical Review Letters 1984; 53: 1951-3.
[2] Senechal M. Quasicrystals and Geometry. New York: Cambridge University Press; 1995
[3] Penrose R. Pentaplexity. Bulletin of the Institute for Mathematics and Applications 1974; 10: 266-271.
[4] Penrose R. Pentaplexity: a class of nonperiodic tilings of the plane. The Mathematical Intelligencer 1979; 2: 32-37.
[5] Coates G. Derivation of the Penrose prototiles. http://www.maths.adelaide.edu.au/MLC/Penrose.html; 2001.
[6] Conway JH, Sloane NJA. Sphere Packings, Lattices, and Groups, 3rd Edition. New York: Springer-Verlag; 1998.
[7] Connes A. Noncommutative Geometry San Diego: Academic Press Inc.; 1994.
[8] El Naschie MS. On the 26-Dimensinal Leech Lattice and E^{∞} Nuclear Space, Chaos, Solitons & Fractals 1999; 10: 1813-1819.
[9] Nottale L. Fractal Space-Time and Microphysics. Singapore: World Scientific Publishing Co.; 1993.
[10] Nottale L. Scale Relativity and Fractal Space-Time: Applications to Quantum Physics, Cosmology and Chaotic Systems. Chaos, Solitons & Fractals 1996;l 7: 877-938.
[11] Ord GN. Fractal Space-Time and the Statistical Mechanics of Random Walks. Chaos, Solitons & Fractals 1996; 7: 821-843.
[12] Hahn T, editor. International Tables for Crystallography, Volume A, 4th edition. Boston, MA: Kluwar Academic Publishers; 1996.
[13] Shmueli U, editor. International Tables for Crystallography, Volume B. Boston, MA: Kluwar Academic Publishers; 1996.
[14] Wilson AJC, Prince E, editors. International Tables for Crystallography, Volume C, 2nd edition. Boston, MA: Kluwar Academic Publishers; 1999.
[15] Brown G, Bülow R, Neubüser J, Wondratschek H, Zassenhaus H. Crystallographic Groups of Four-Dimensional Space. New York: John Wiley & Sons; 1978.
[16] Harburn G, Taylor CA Welberry TR. Atlas of Optical Transforms. London: G. Bells & Sons, Ltd; 1972.
[17] Grünbaum B and Shepard G. Tilings and Patterns. New York: W H Freeman; 1987.
[18] Radin C. Miles of Tiles. Providence, RI: American Mathematical Society; 1999.
[19] Ammann, R., Grünbaum B and Shepard G. Aperiodic Tiles. Discrete & Computational Geometry 1992; 8: 1-25.
[20] Lewis AD. Quasicrystal Picture Gallery. http://penelope.mast.queensu.ca/~andrew/qc/; 1998.

[21] Baake M, Kramer P, Schlottmann M and Zeidler D. Planar Patterns with Fivefold symmetry as Sections of Periodic Structures in 4-space. International Journal of Modern Physics B 1990; 4: 2217-68.
[22] Gähler P and Stampfli F. The dualisation method revisted: Dualisation of product Laguerre complexes as a unifying framework. International Journal of Modern Physics B 1993; 7:1333-49 .
[23] Schlottmann M. Periodic and quasiperiodic Laguerre tilings. International Journal of Modern Physics B 1993; 7: 1351-62.
[24] Thang L T, Piunikhin S and Sadov V. Local Rules for Quasiperiodic Tilings. Communications in Mathematical Physics 1992; 150: 23-44.
[25] Thang L T and Piunikhin S. Local rules for multi-dimensional quasicrystals. Differential Geometry and its Applications 1995; 5: 13-31.
[26] Oguey C, Duneau M and Katz A. A geometrical approach of Quasiperiodic Tilings. Commun. Math Physics 1988; 118: 99-118.
[27] Coxeter HSM. Regular Polytopes, 3rd edition. New York: Dover Publications, Inc. 1973.
[28] Reiter CA. Web addendum to atlas of quasicrytalline tilings. http://www.lafayette.edu/~reiterc/aqct/index.html; 2001.
[29] Reiter CA. Fractals, Visualization and J, 2nd edition. Toronto: Jsoftware, Inc; 2000.
[30] Allis NW, Dumont JP and Reiter CA. Visualizing point sets, fractals, and quasicrystals using raster techniques. Computers & Graphics 2001; 25: 519-527.
[31] Jsoftware. http://www/jsoftware.com; 2001.

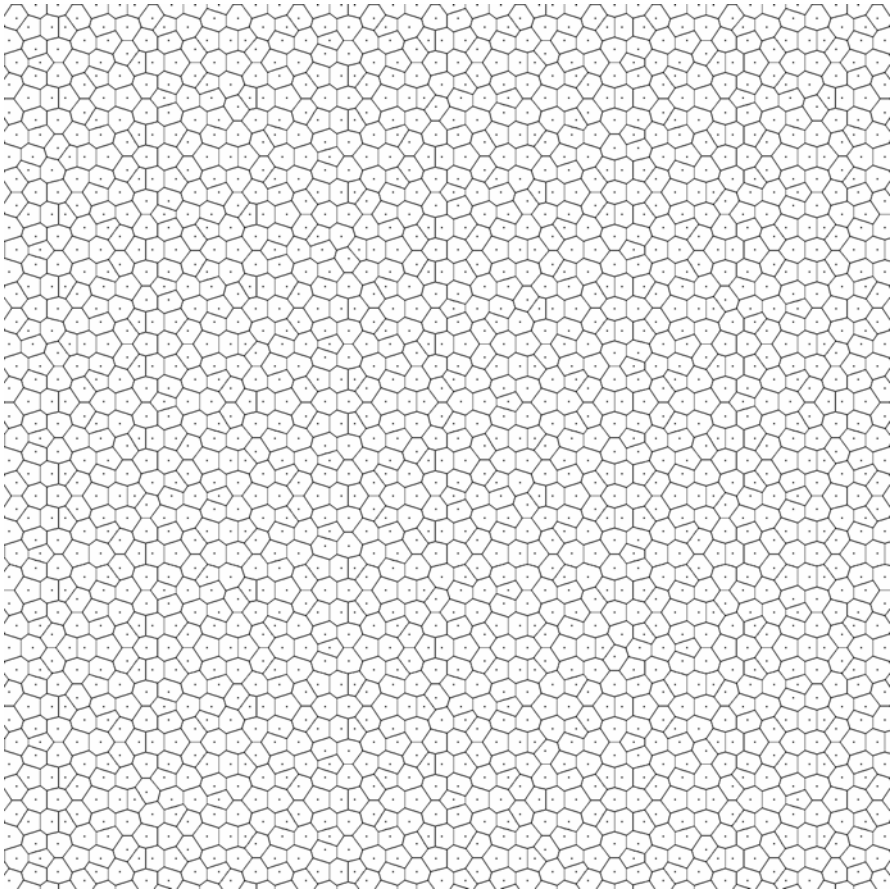

Figure 1. Voronoi Cells around a Penrose point collection.

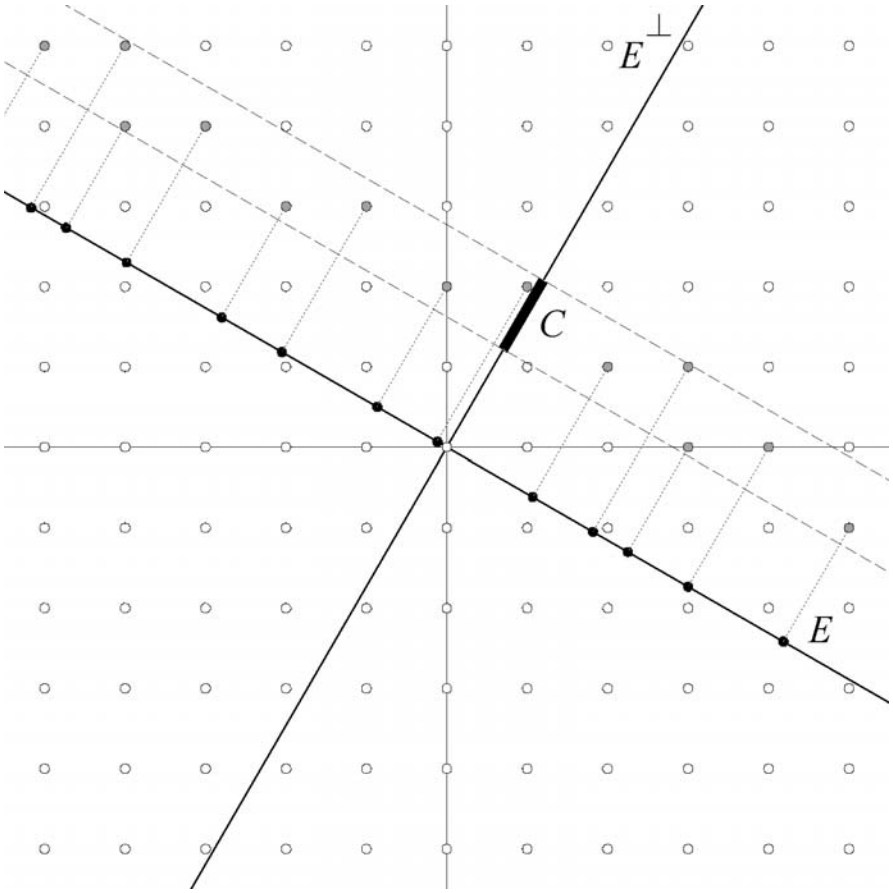

Figure 2. Canonical projection in a simple case.

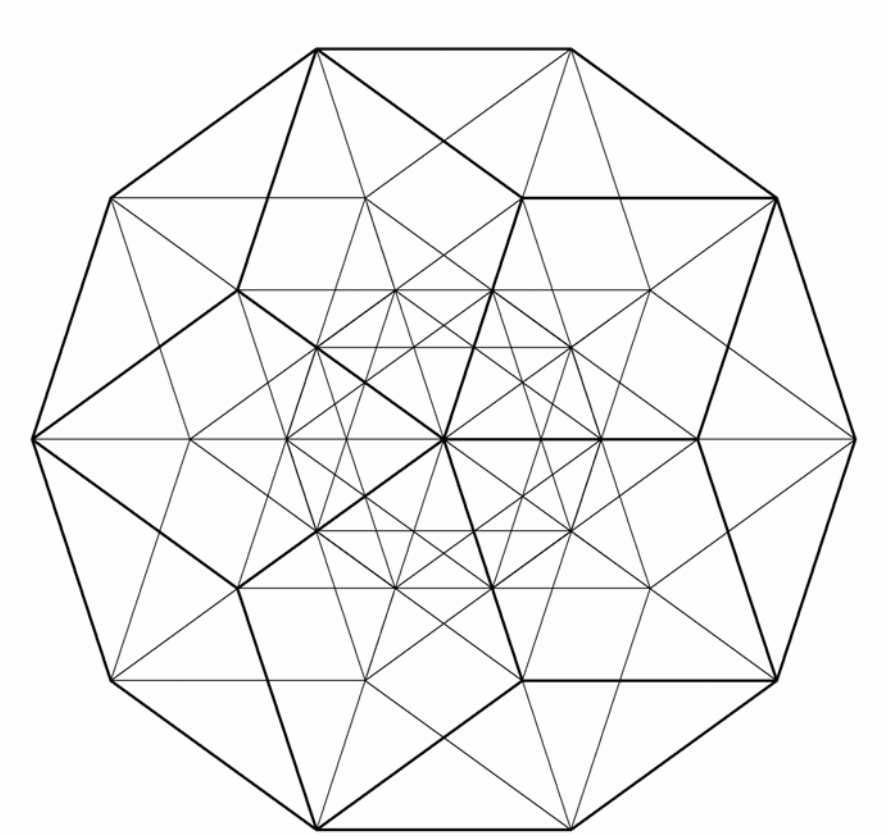

Figure 3. Projection of a 5-dimensional cube.

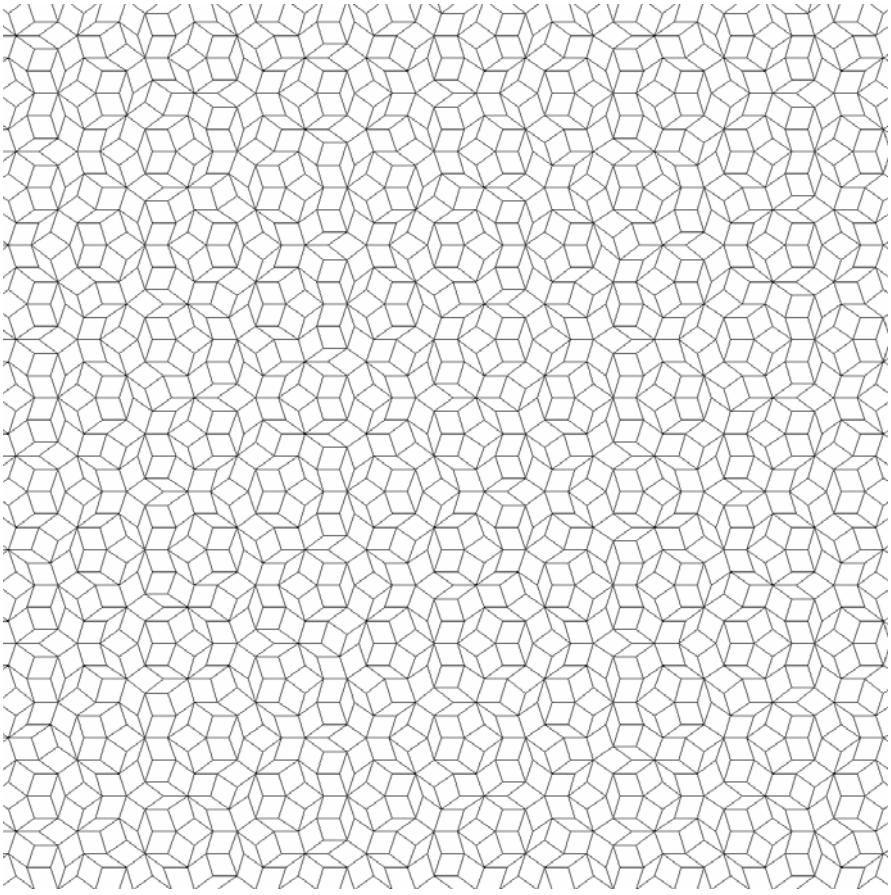

Figure 4. A Penrose tiling using an s_1 shift of the Voronoi cell.

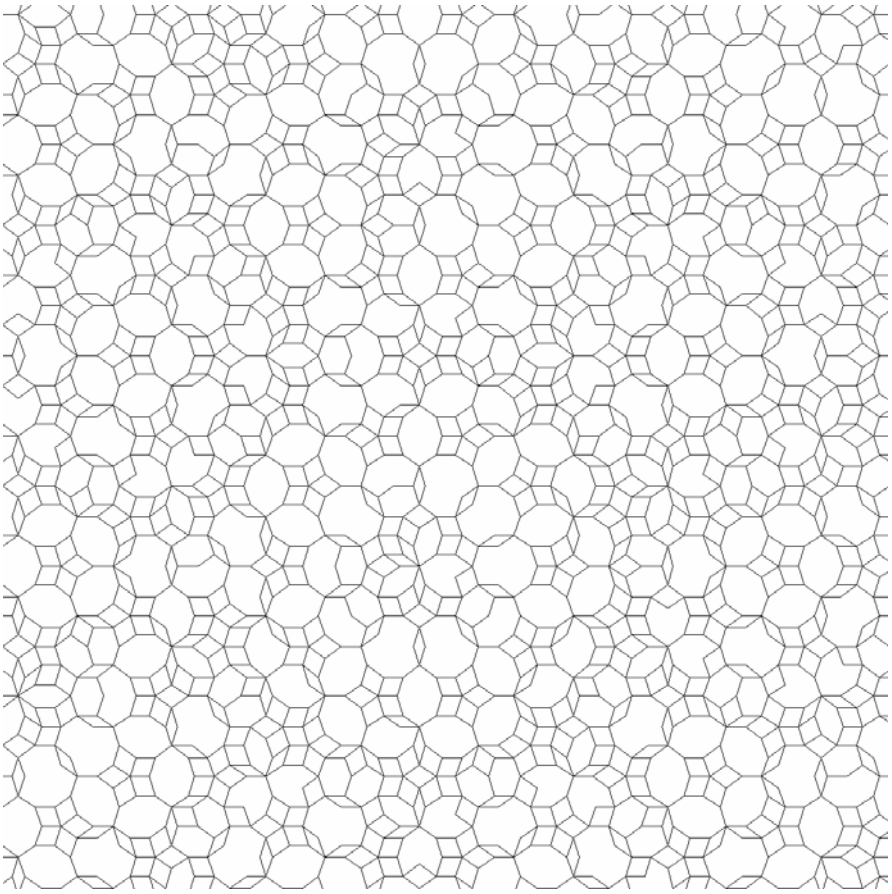

Figure 5. Tiling when the Voronoi cell is contracted by 0.9.

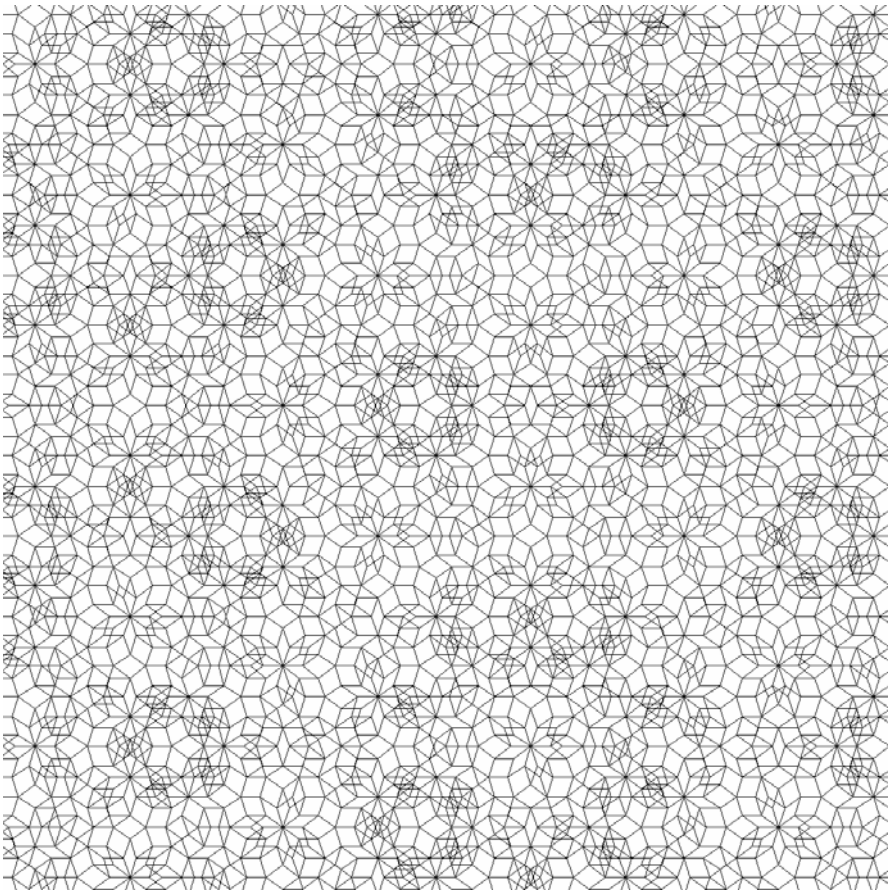

Figure 6. Tiling when the Voronoi cell is expanded by 1.1.

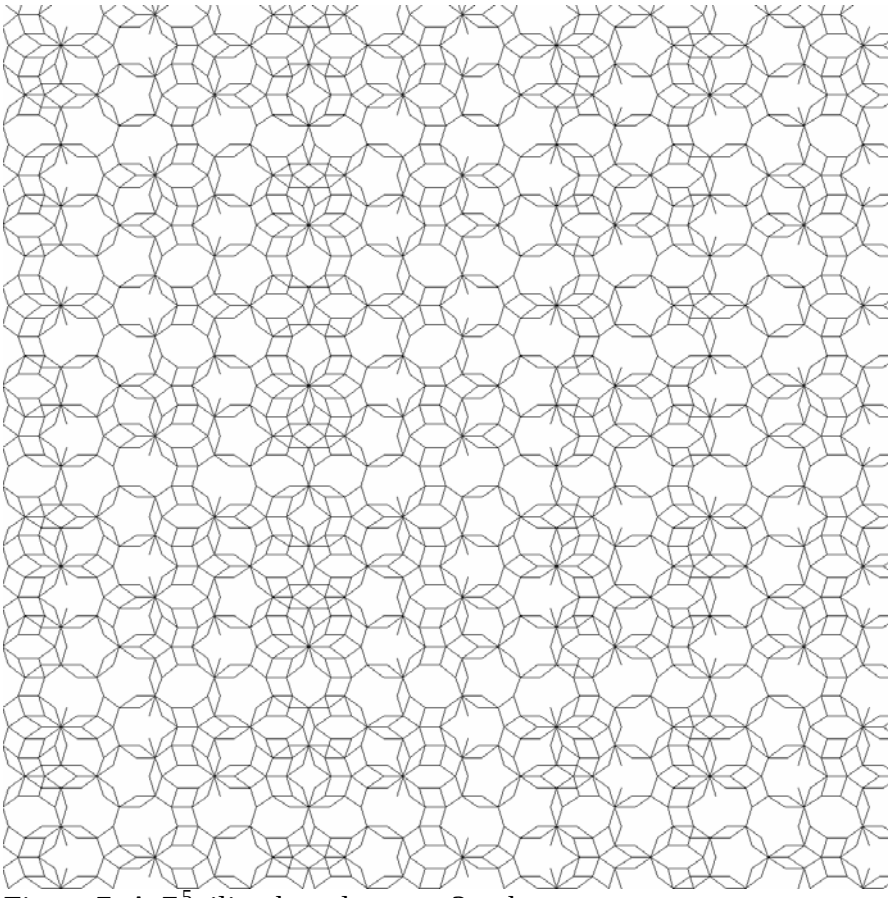

Figure 7. A Z^5 tiling based upon a 3-cube.

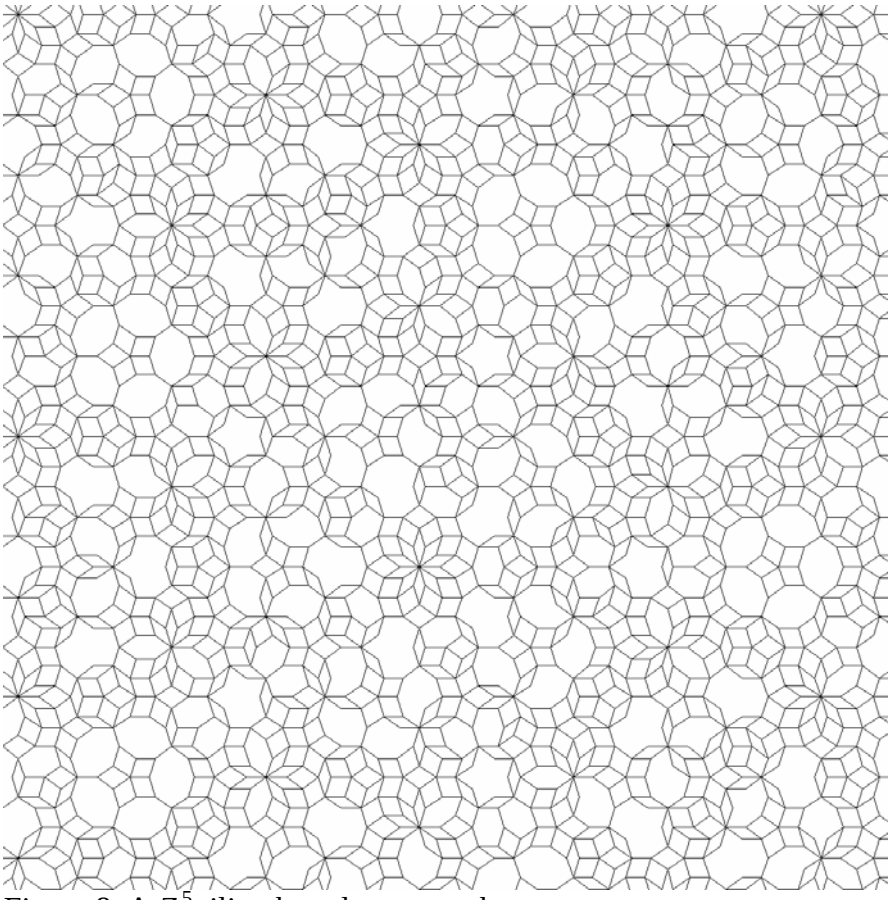

Figure 8. A Z^5 tiling based upon a sphere.

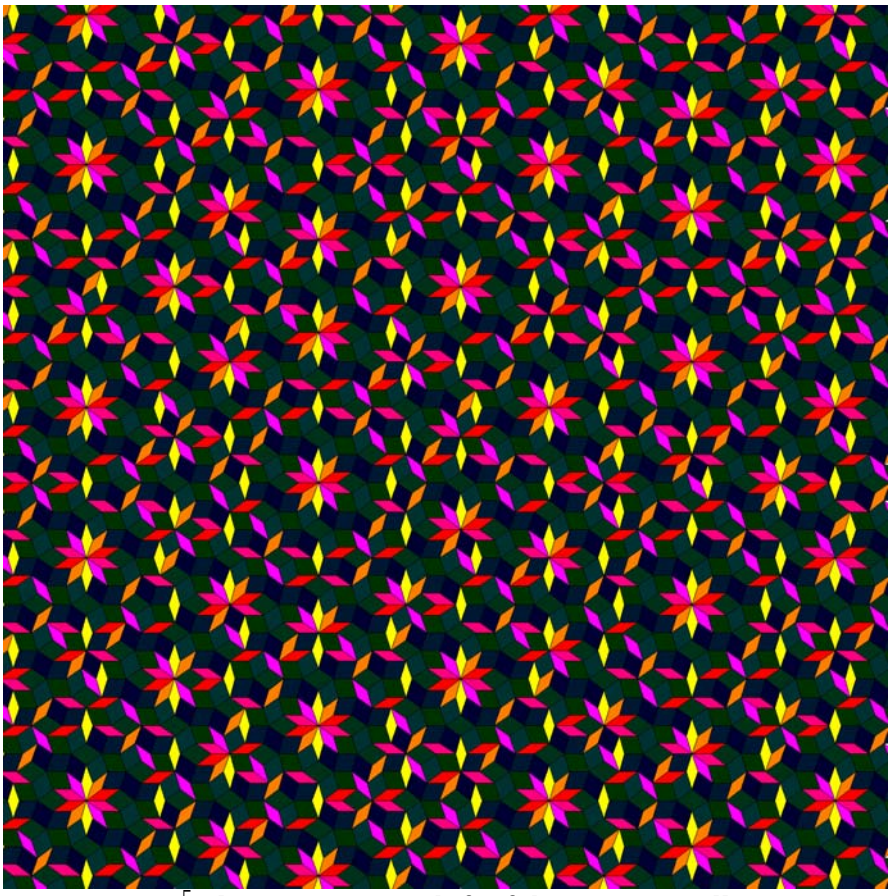

Figure 9. A Z^5 tiling using an s_0 shift of the Voronoi cell.

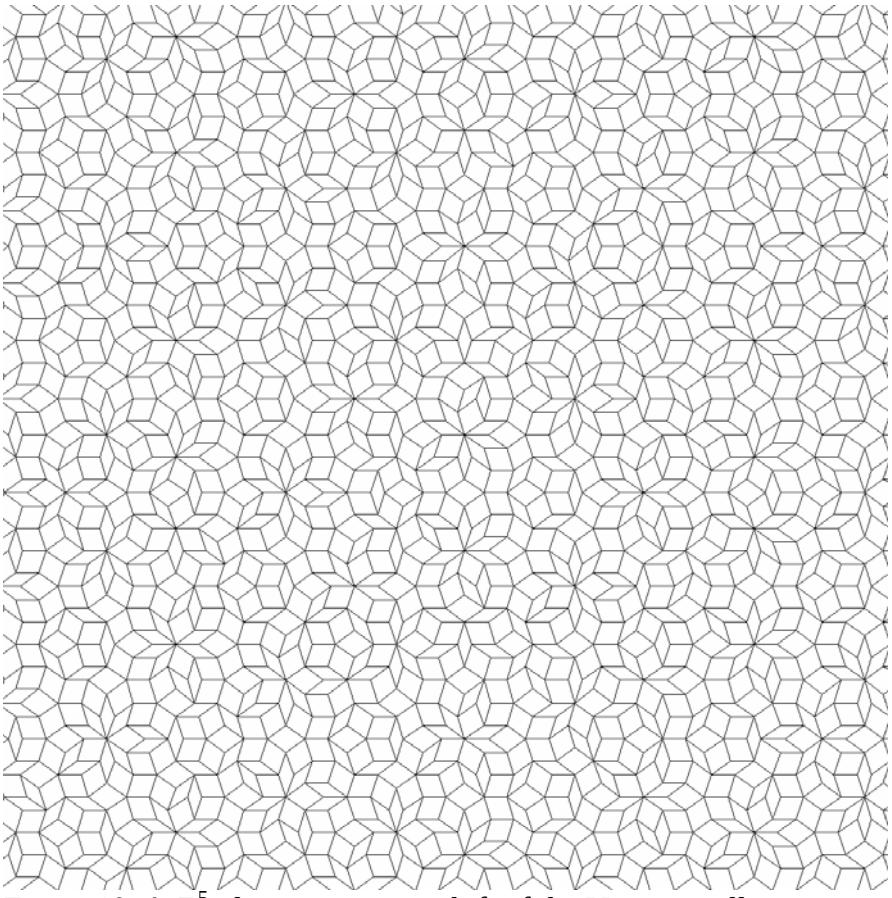

Figure 10. A Z^5 tiling using an s_2 shift of the Voronoi cell.

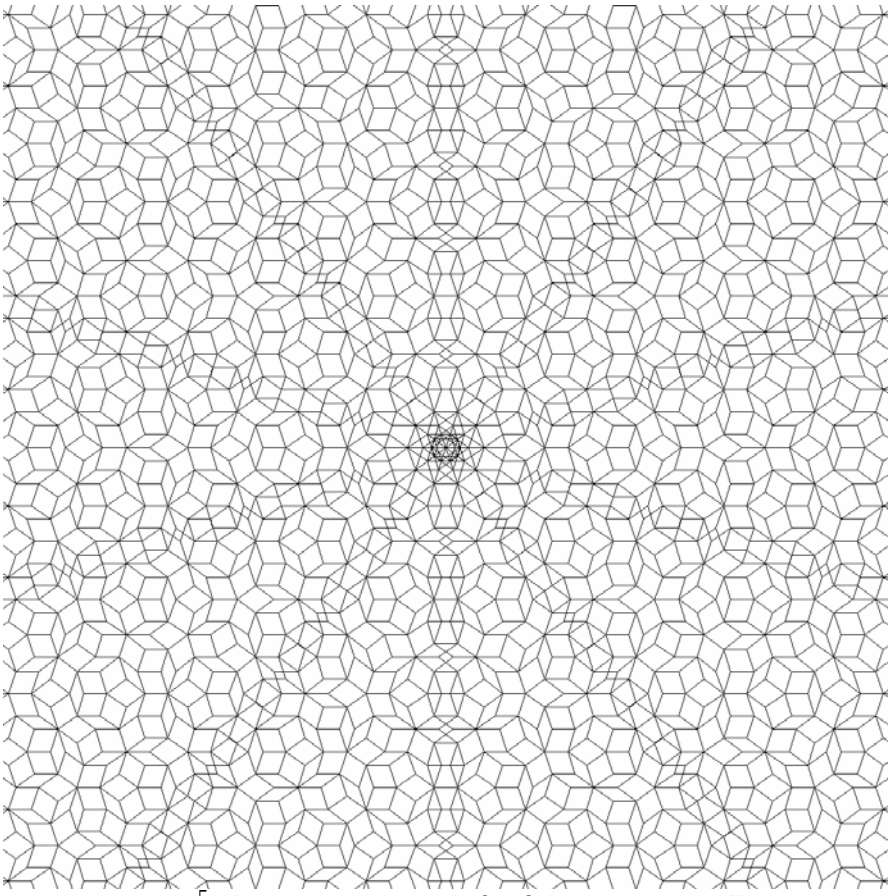

Figure 11. A Z^5 tiling using an s_3 shift of the Voronoi cell.

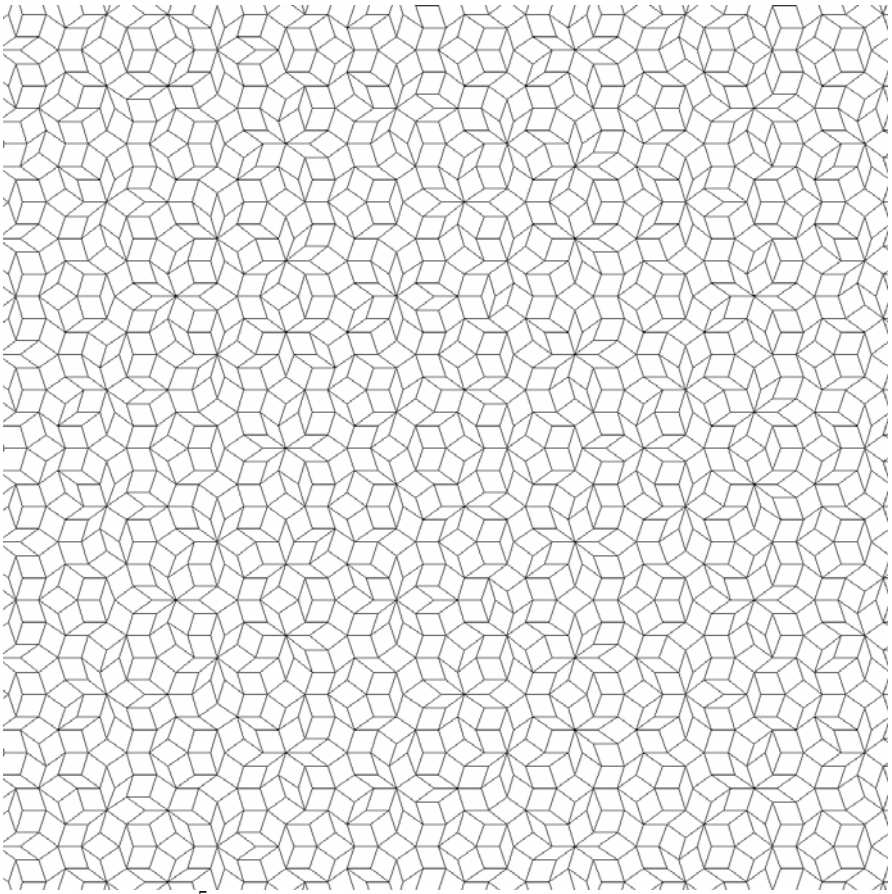

Figure 12. A Z^5 tiling using an s_4 shift of the Voronoi cell.

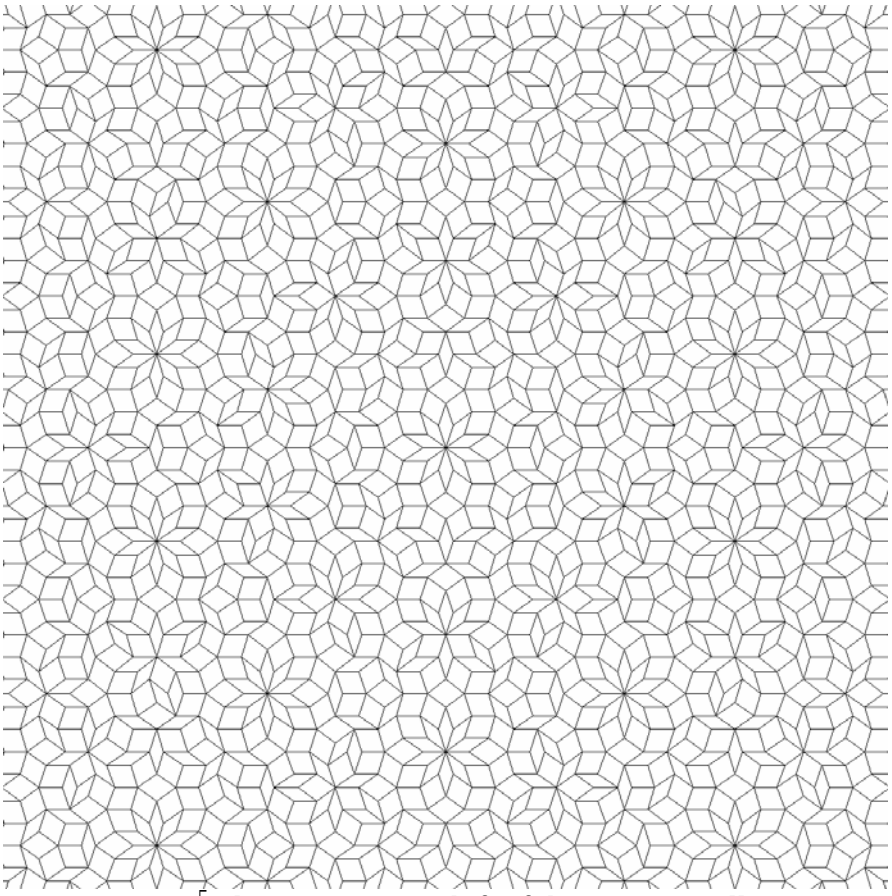

Figure 13. A Z^5 tiling using an s_5 shift of the Voronoi cell.

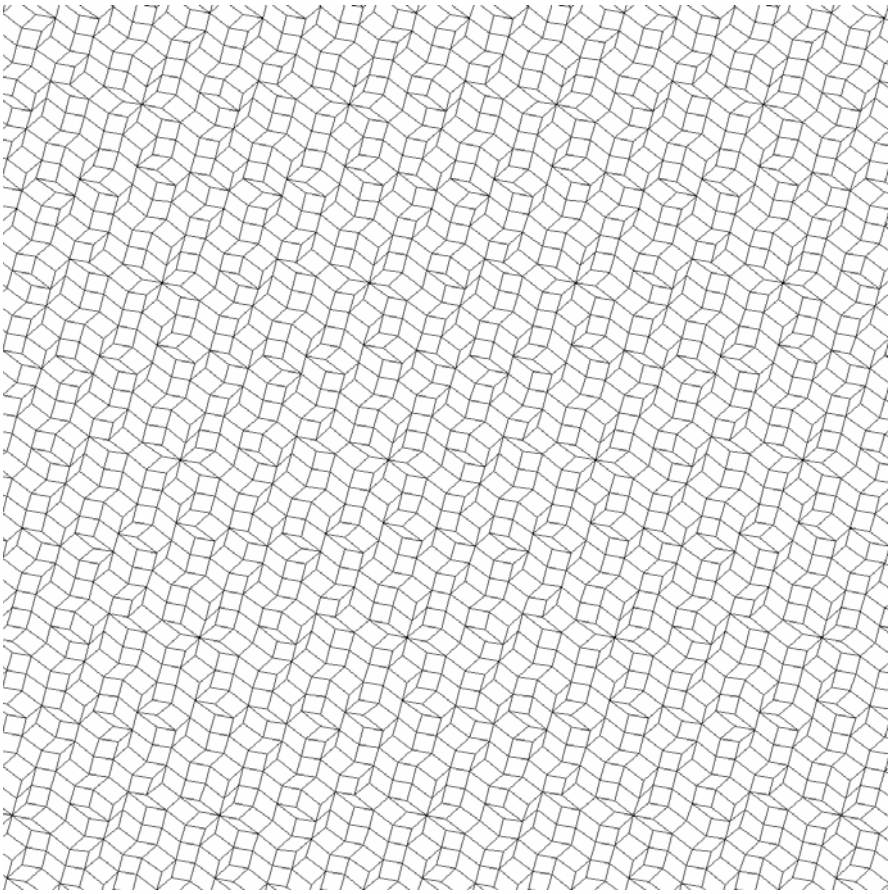

Figure 14. A Z^5 tiling using a random choice for subspaces E and $E^{\perp}$.

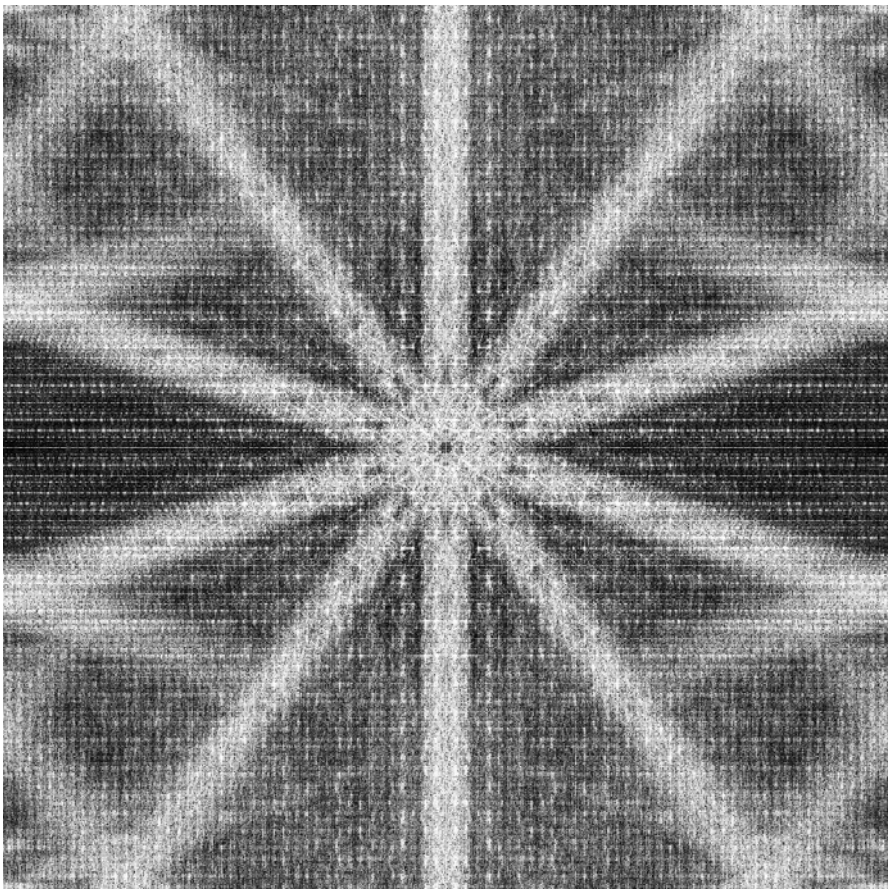

Figure 15. The diffraction pattern with optimized contrast for the tiling in Figure 4.

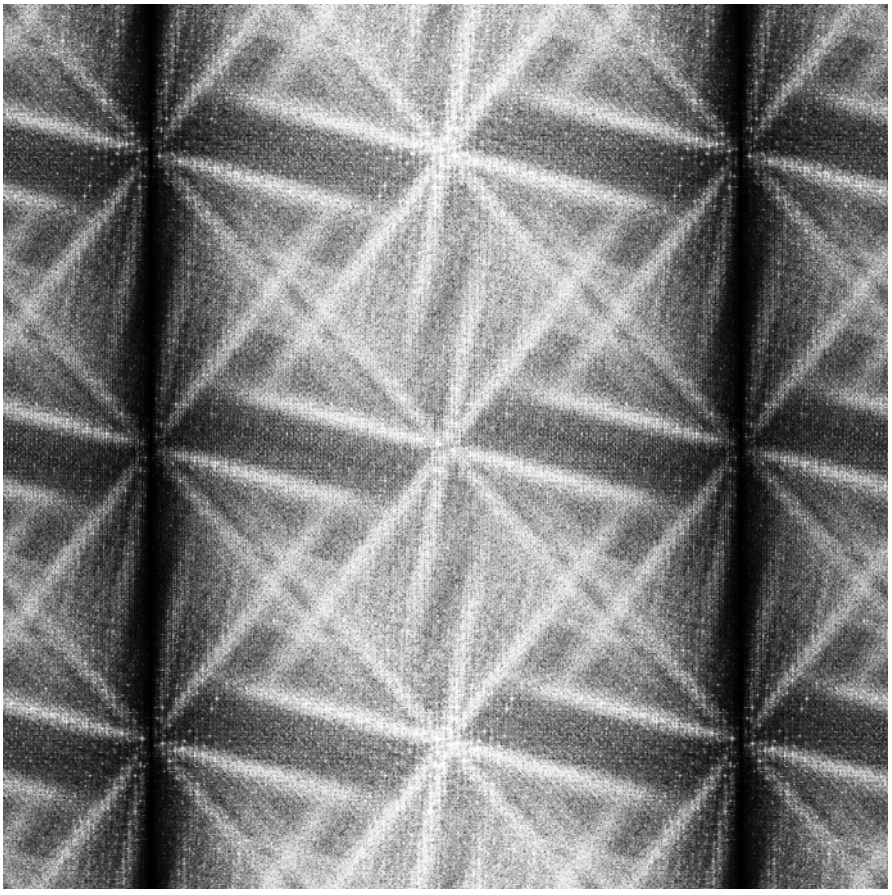

Figure 16. The diffraction pattern with optimized contrast for the tiling in Figure 14.

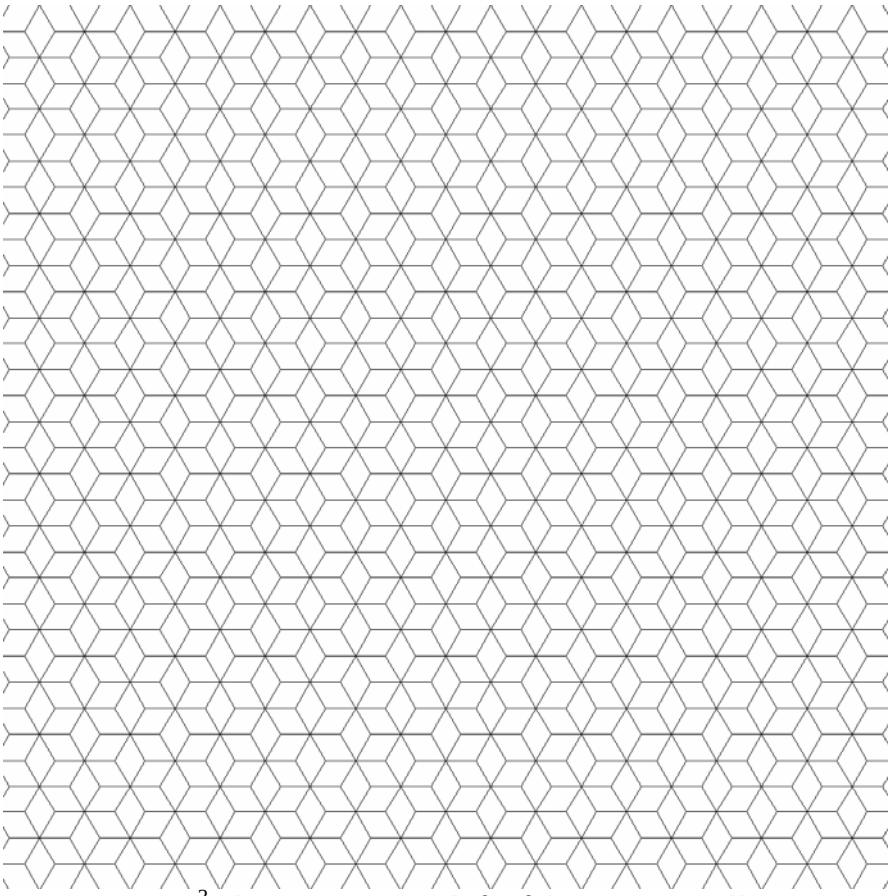

Figure 17. A Z^3 tiling using an s_0 shift of the Voronoi cell.

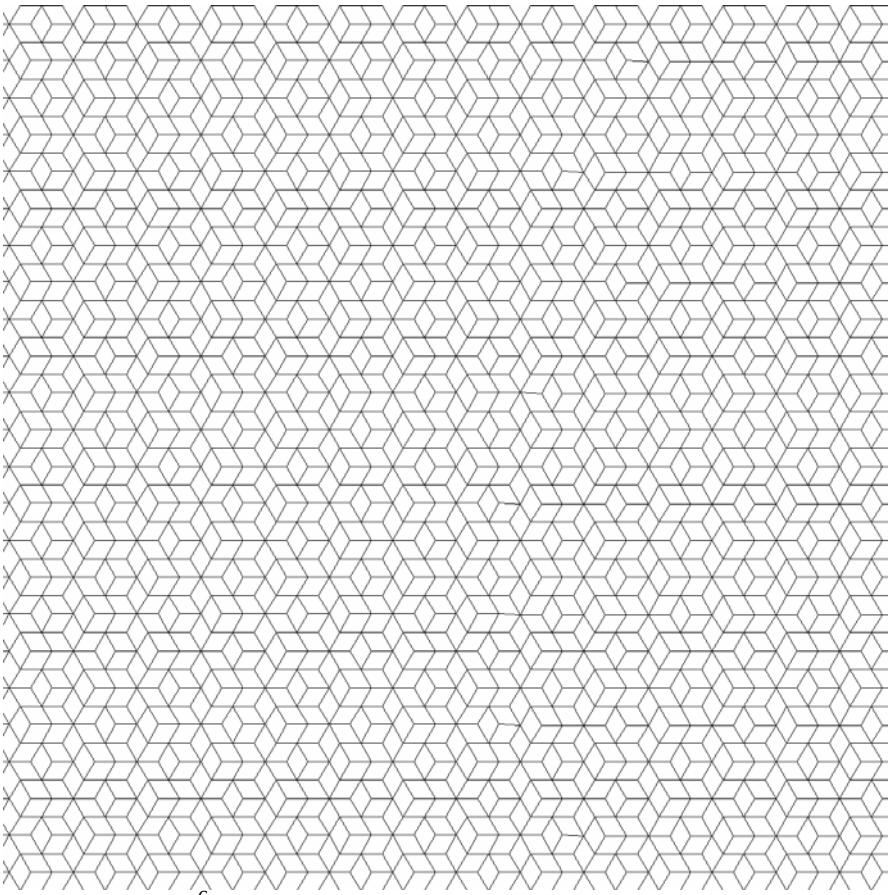

Figure 18. A Z^6 tiling using an s_0 shift of the Voronoi cell.

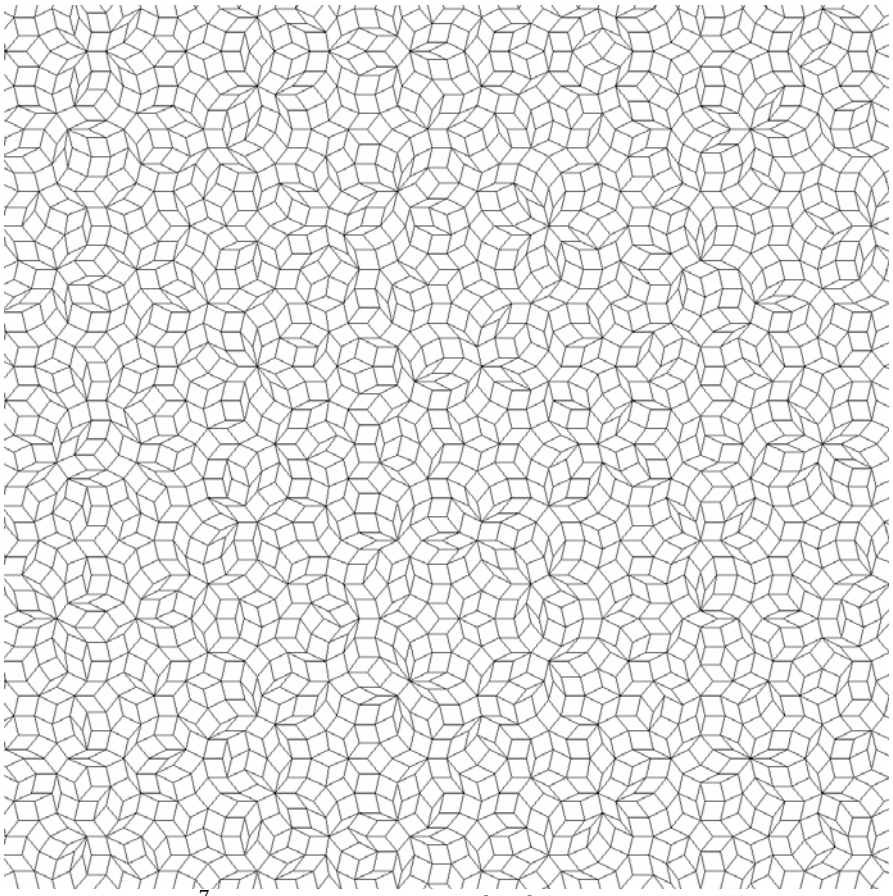

Figure 19. A Z^7 tiling using an s_0 shift of the Voronoi cell.

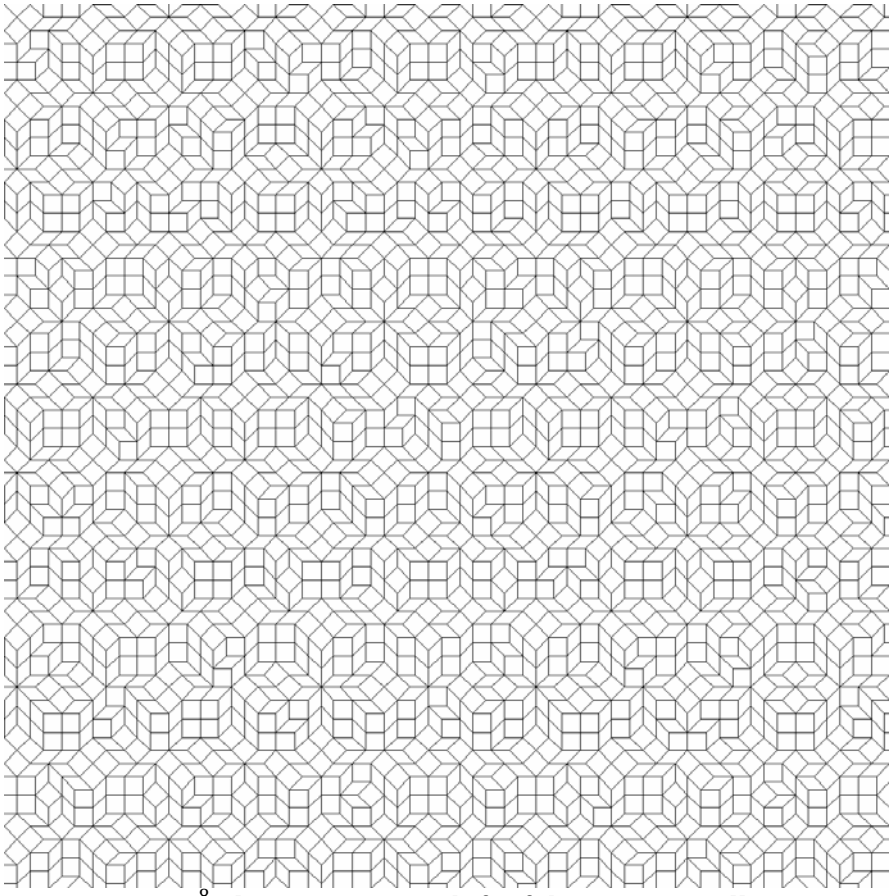

Figure 20. A Z^8 tiling using an s_0 shift of the Voronoi cell.

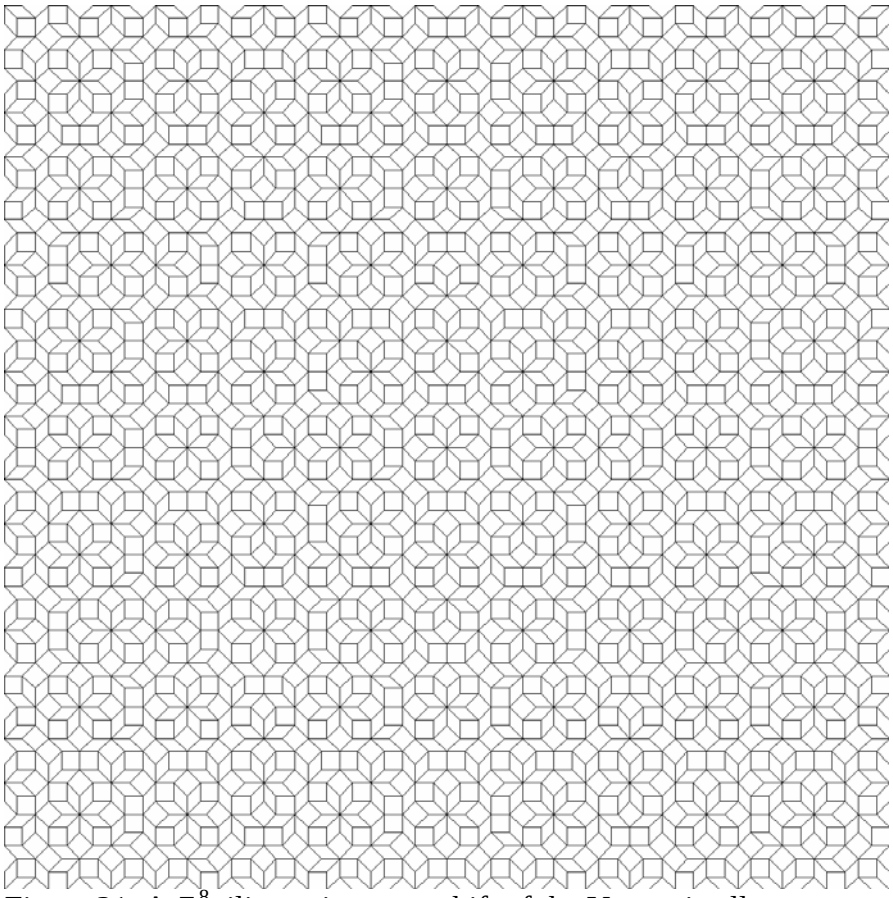

Figure 21. A Z^8 tiling using an s_4 shift of the Voronoi cell.

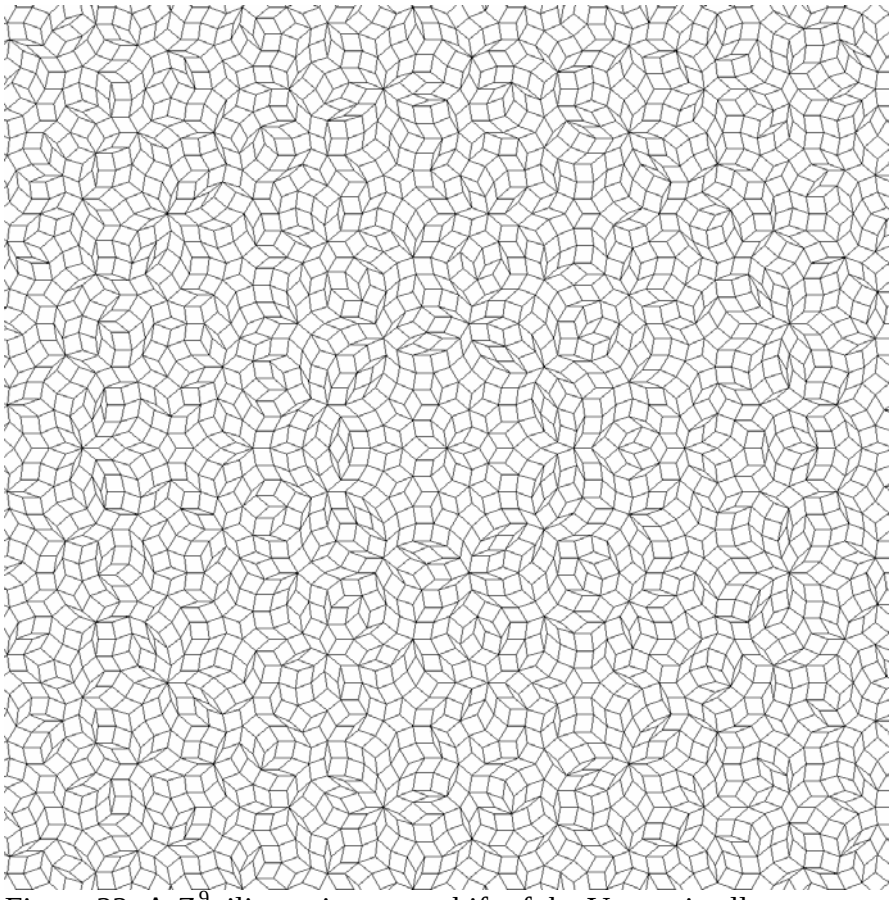

Figure 22. A Z^9 tiling using an s_4 shift of the Voronoi cell.

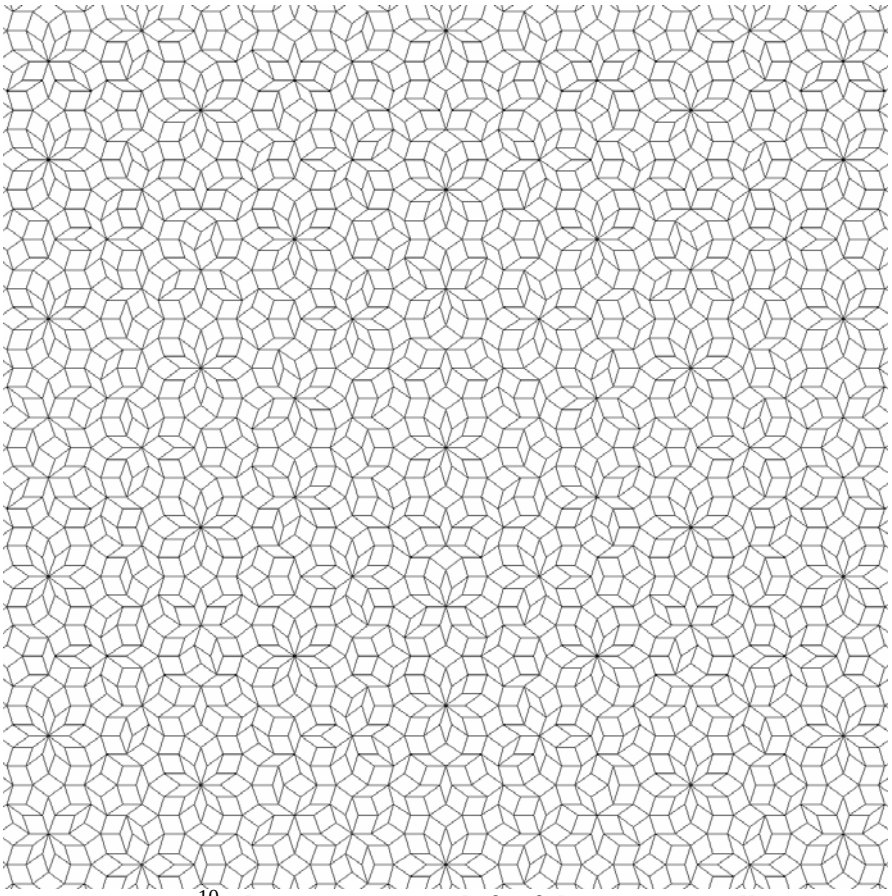

Figure 23. A Z^{10} tiling using an s_4 shift of the Voronoi cell.

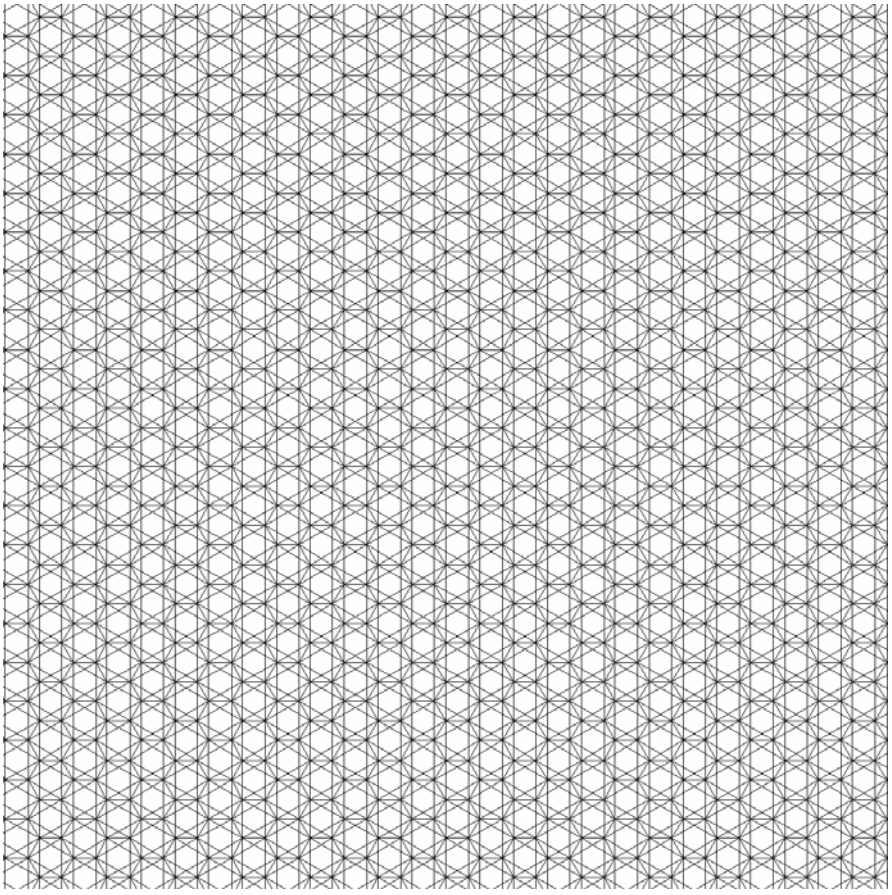

Figure 24. A D_3 tiling using an s_0 shift of the Voronoi cell.

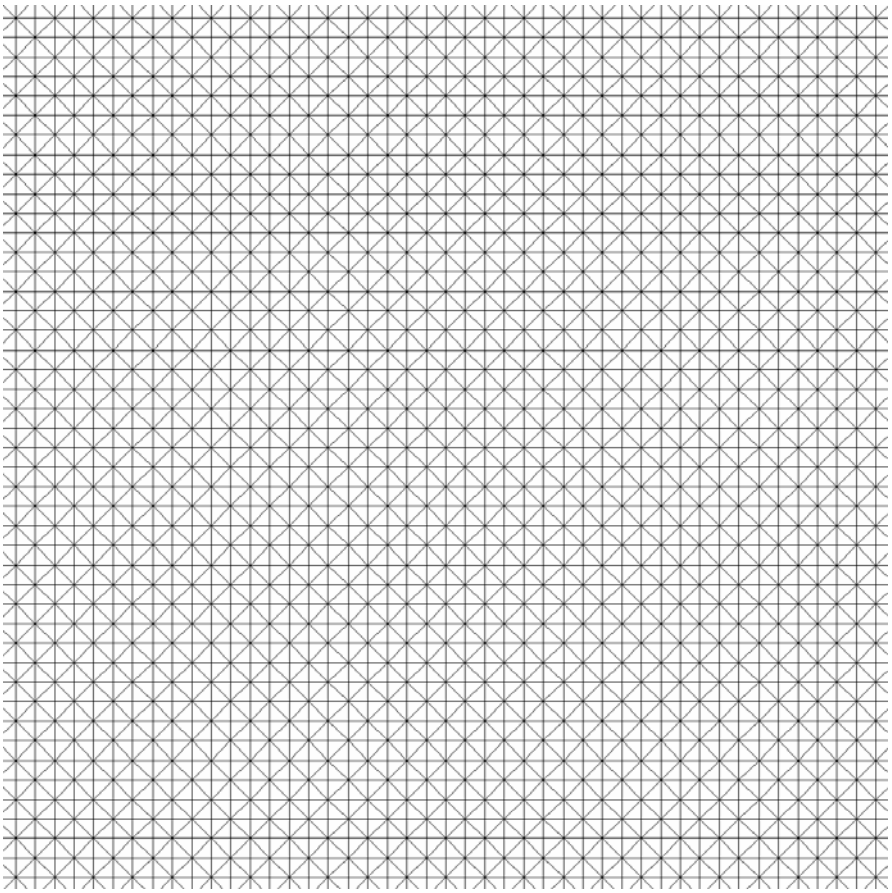

Figure 25. A D_4 tiling using an s_0 shift of the Voronoi cell.

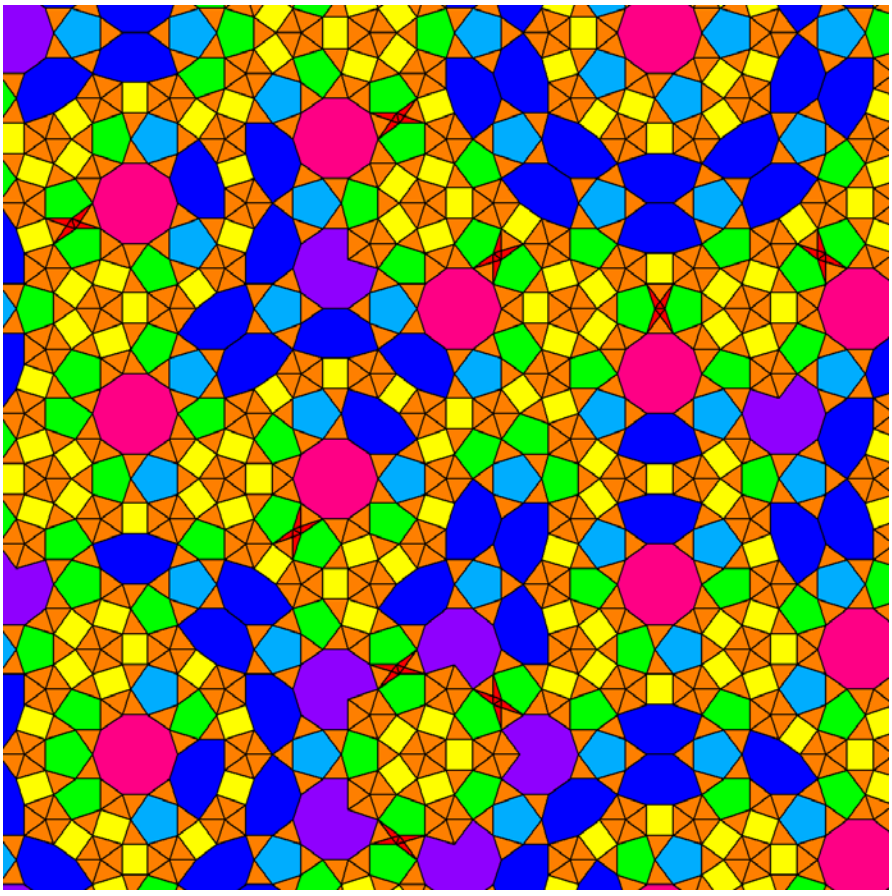

Figure 26. A D_5 tiling using an s_0 shift of the Voronoi cell.

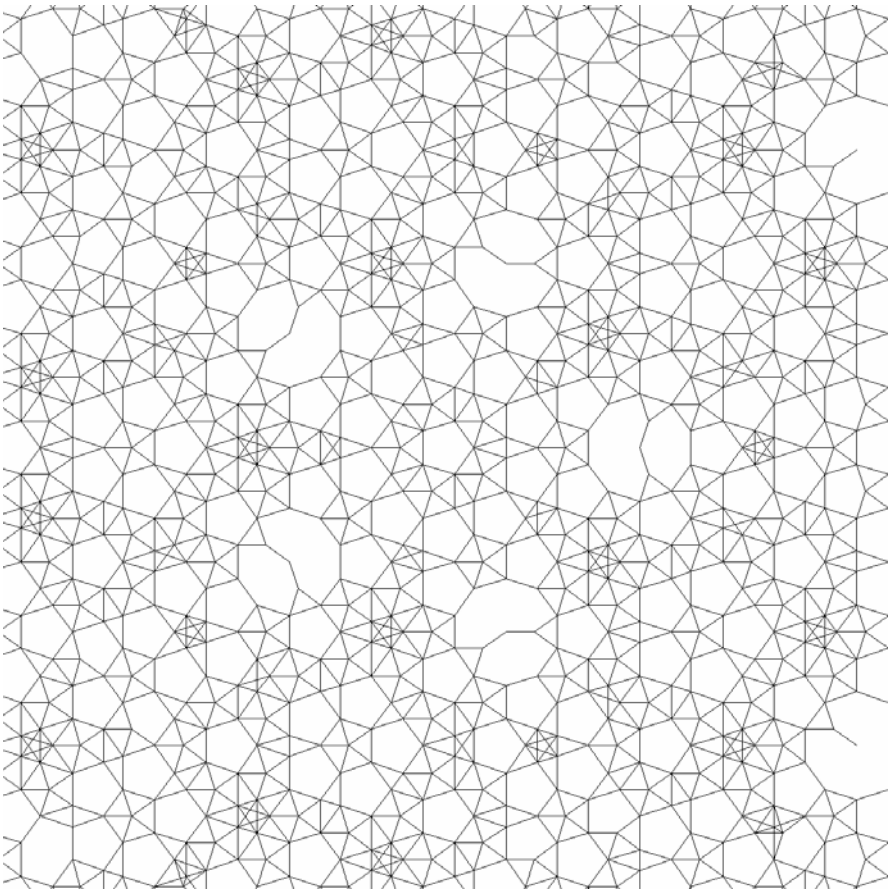

Figure 27. A D_5 tiling using an s_3 shift of the Voronoi cell.

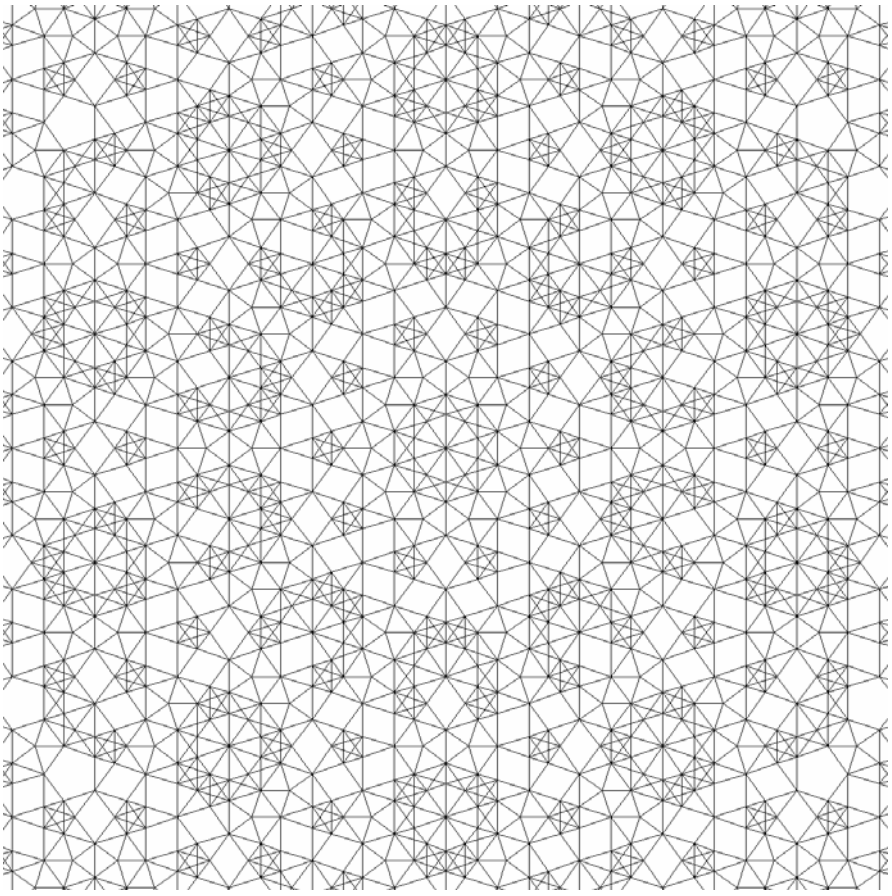

Figure 28. A D_5 tiling using an s_5 shift of the Voronoi cell.

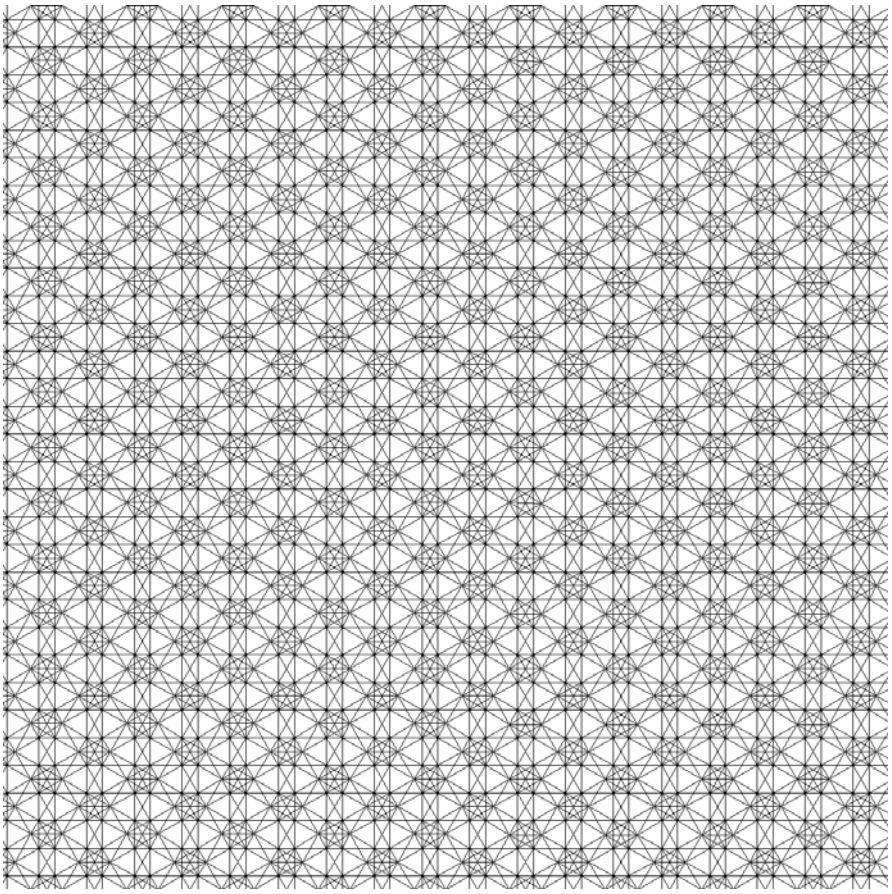

Figure 29. A D_6 tiling using an s_1 shift of the Voronoi cell.

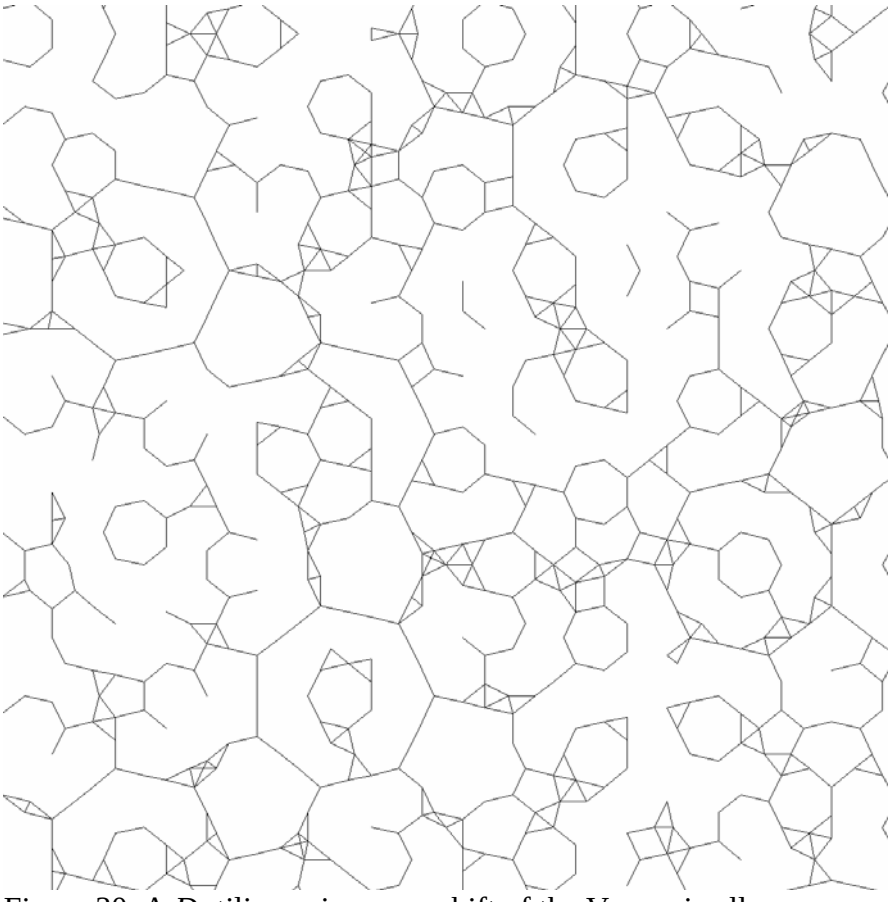

Figure 30. A D_7 tiling using an s_1 shift of the Voronoi cell.

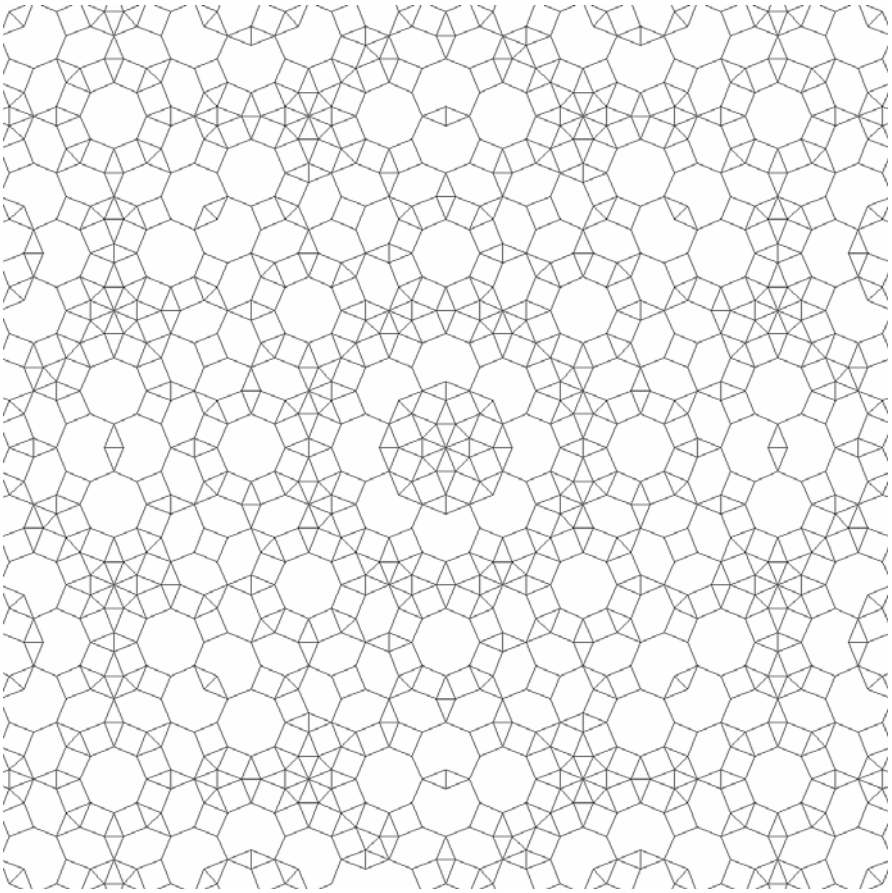

Figure 31. A D_8 tiling using an s_3 shift of the Voronoi cell.

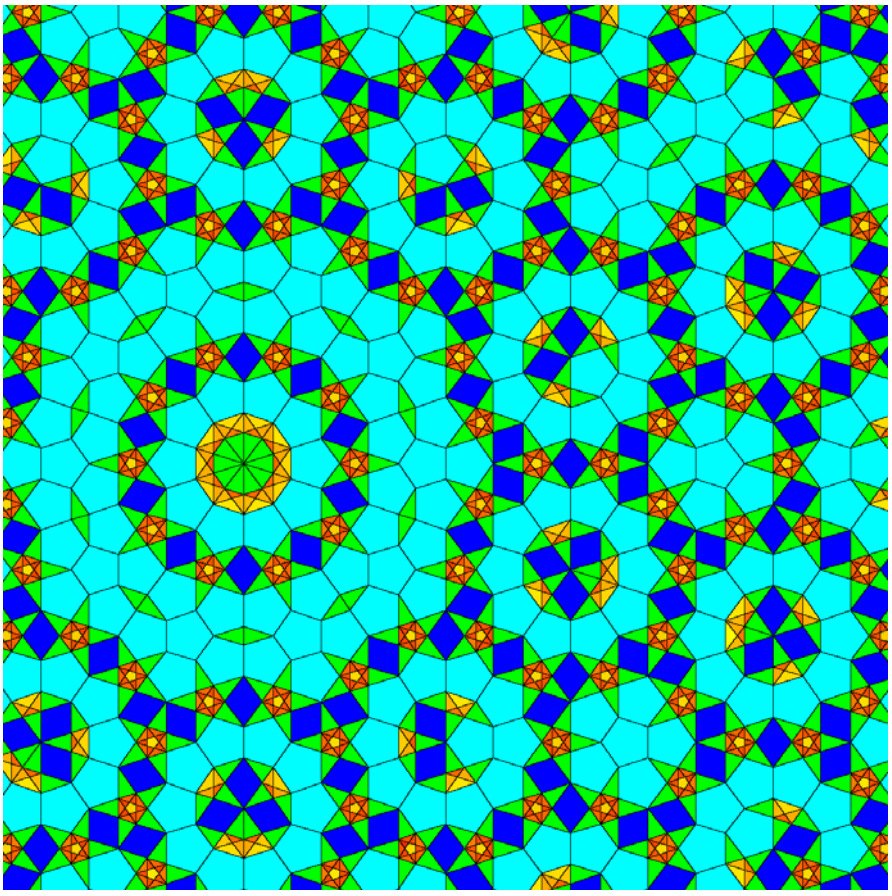

Figure 32. An A_4 tiling using an s_0 shift and 0.5 contraction of the Voronoi cell.

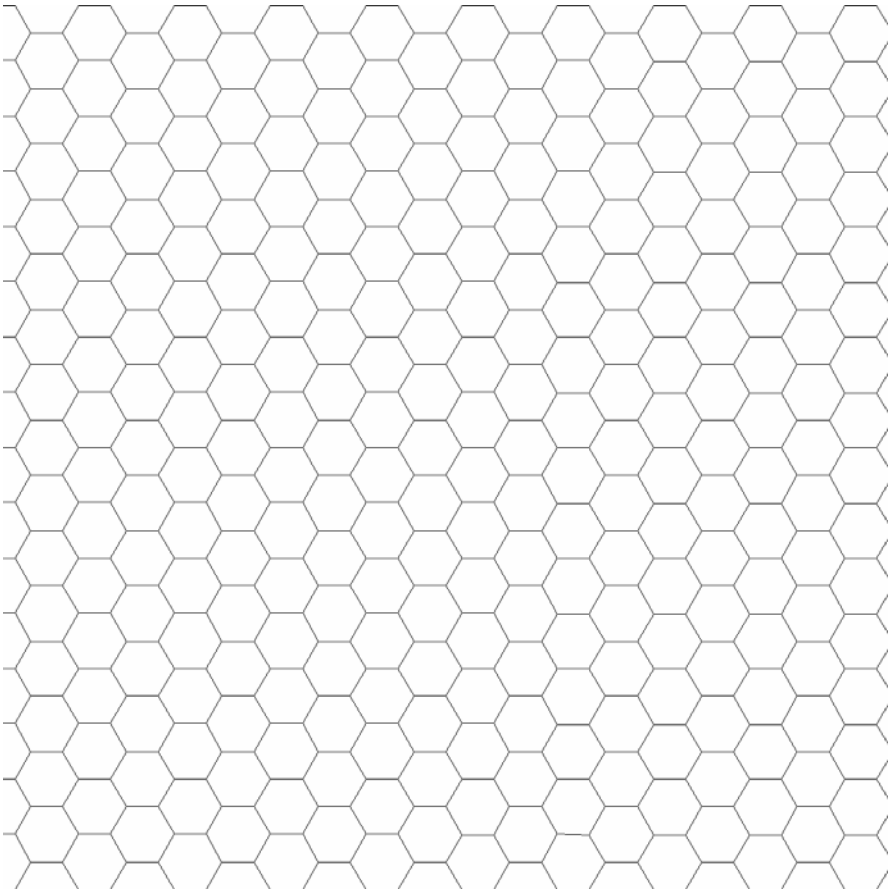

Figure 33. An A_5 tiling using an s_0 shift of the Voronoi cell.

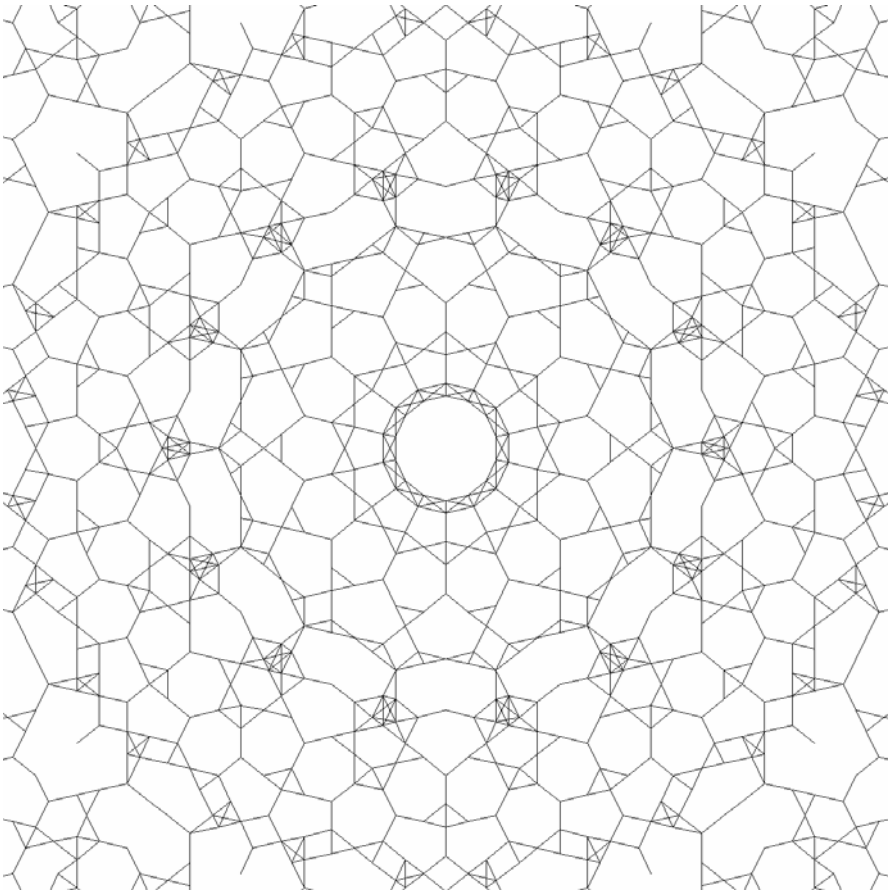

Figure 34. An A_6 tiling using an s_5 shift of the Voronoi cell.

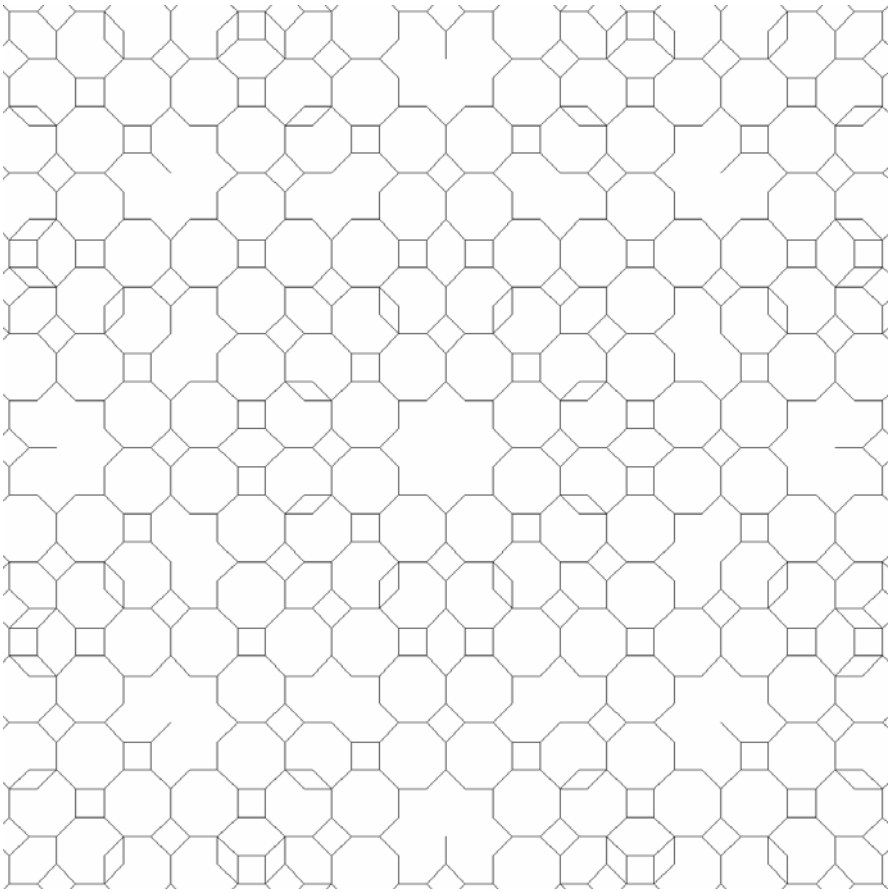

Figure 35. An A_7 tiling using an s_5 shift and a 1.1 expansion of the Voronoi cell.

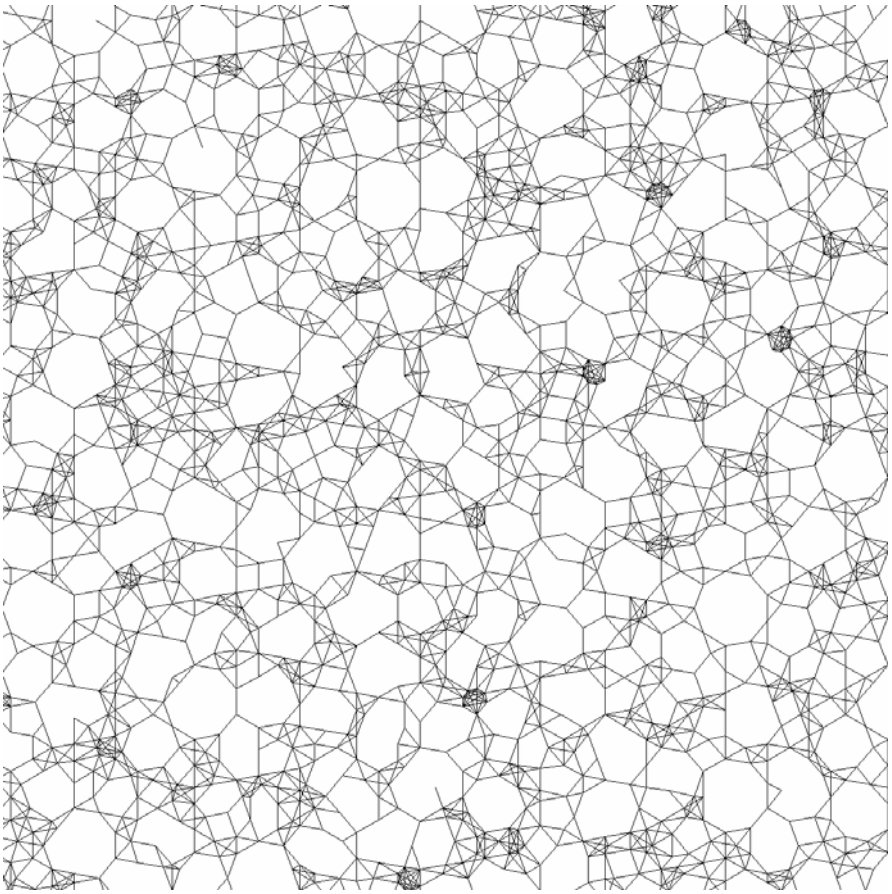

Figure 36. An A_8 tiling using an s_0 shift and a 1.2 expansion of the Voronoi cell.

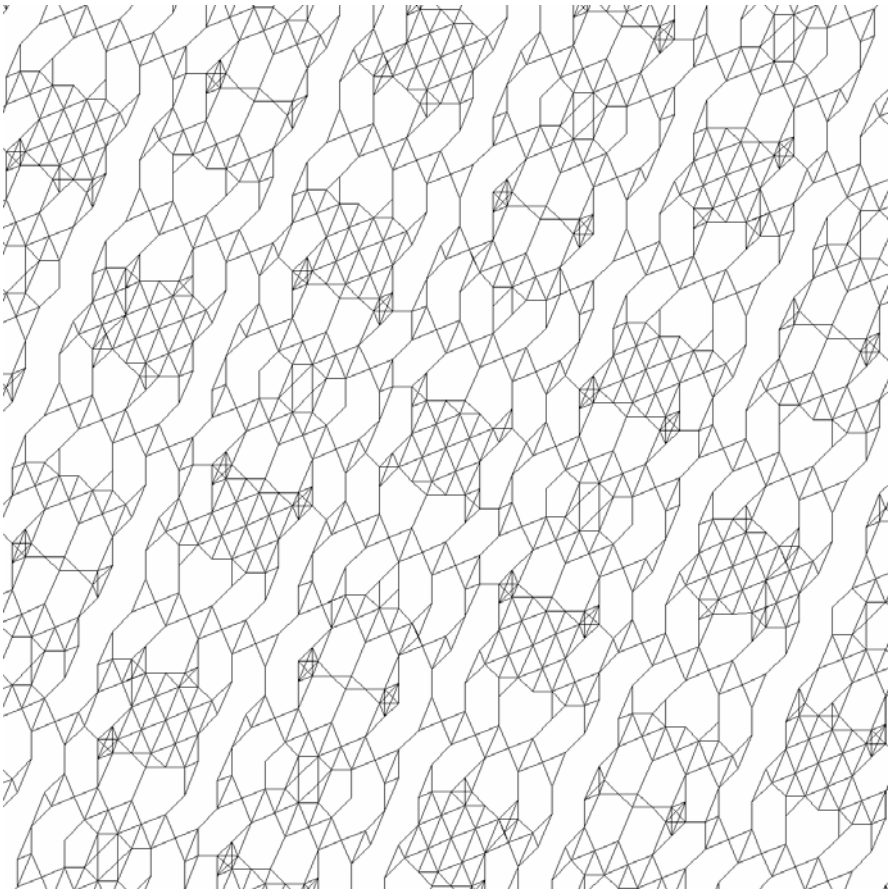

Figure 37. An E_6 tiling using an s_3 shift and a 1.9 expansion of the Voronoi cell.

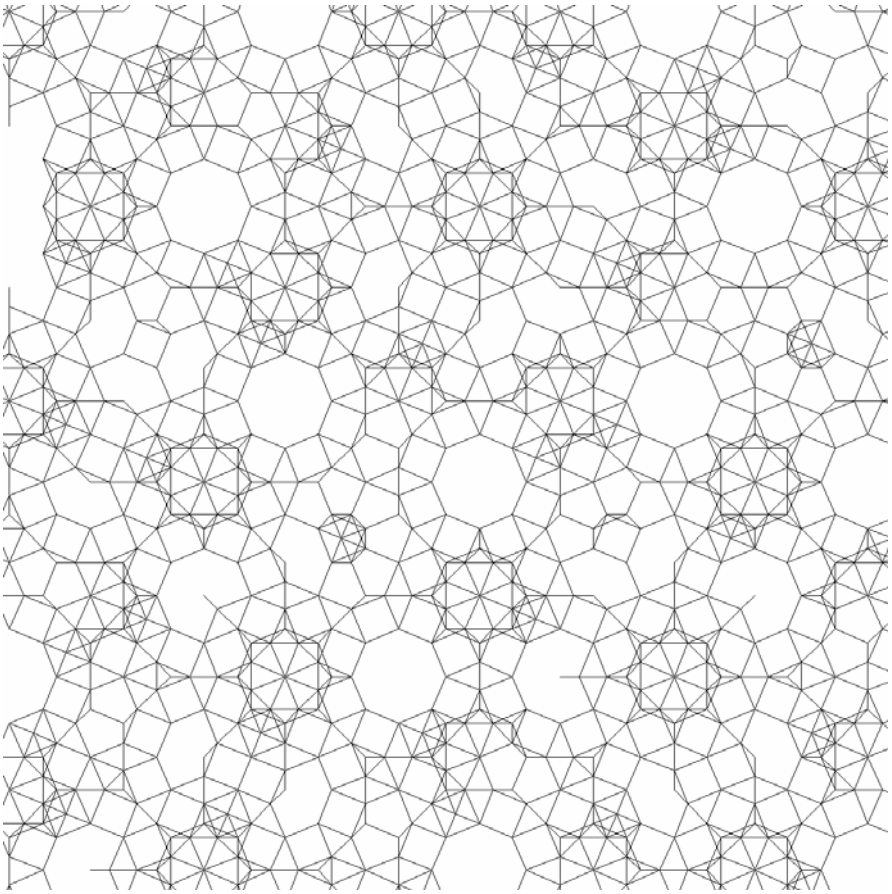

Figure 38. An E_7 tiling using an s_2 shift and a 1.9 expansion of the Voronoi cell.

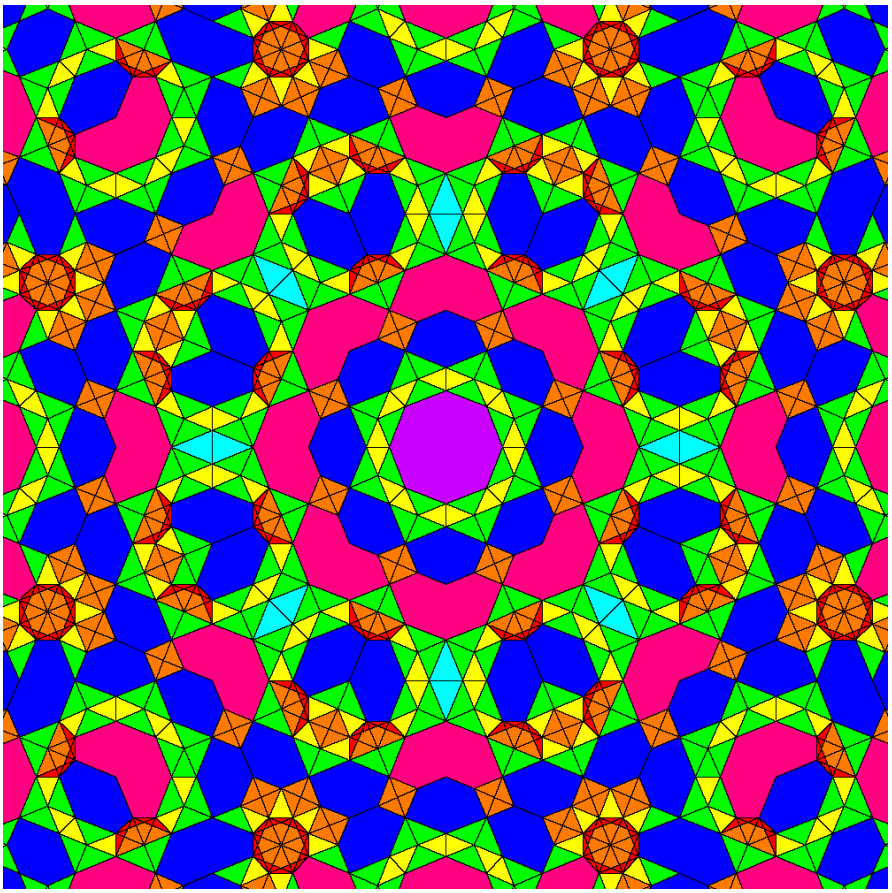

Figure 39. An E_8 tiling using an s_3 shift and a 2.0 expansion of the Voronoi cell.

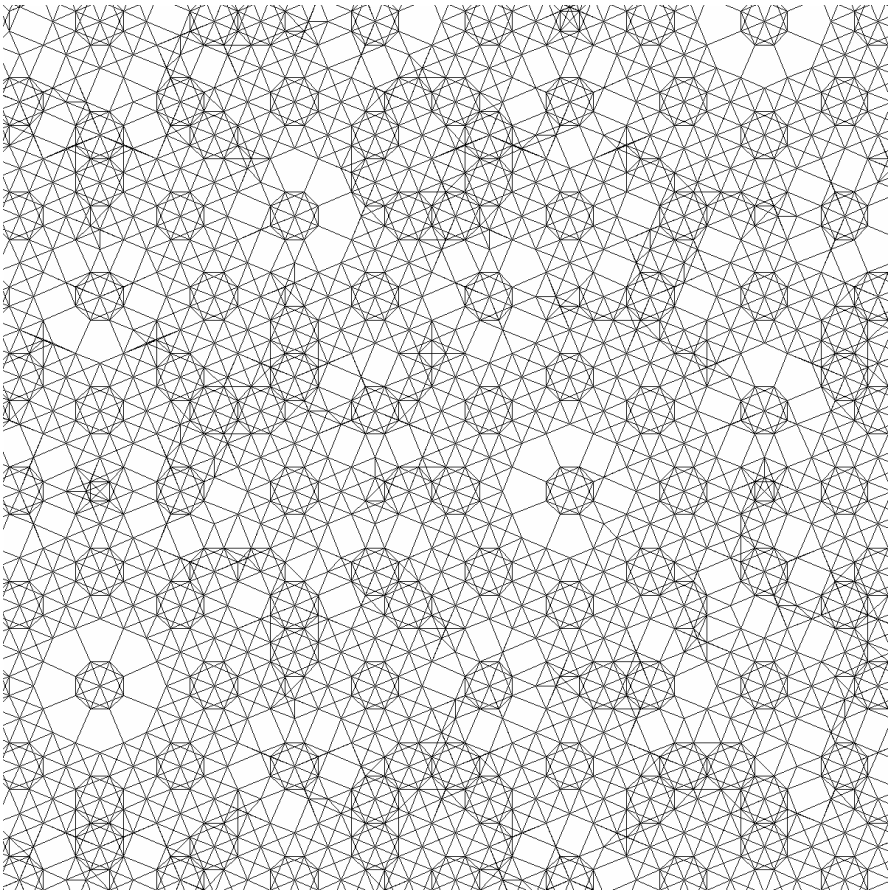

Figure 40. An E_8 tiling using an s_2 shift and a 2.15 expansion of the Voronoi cell.